Methylammonium cation dynamics in methylammonium lead halide perovskites: a solid-state NMR perspective

Bernard, Guy M.; Wasylishen, Roderick E.; Ratcliffe, Christopher I.; Terskikh, Victor; Wu, Qichao; Buriak, Jillian M.; Hauger, Tate

Publisher's version / Version de l'éditeur:
https://doi.org/10.1021/acs.jpca.7b11558
The Journal of Physical Chemistry A, 122, 6, pp. 1560-1573, 2018-01-16

THE JOURNAL OF PHYSICAL CHEMISTRY A

Article

Cite This: J. Phys. Chem. A 2018, 122, 1560−1573

pubs.acs.org/JPCA

Methylammonium Cation Dynamics in Methylammonium Lead Halide Perovskites: A Solid-State NMR Perspective

Guy M. Bernard,[†] Roderick E. Wasylishen,*[,†] Christopher I. Ratcliffe,[‡] Victor Terskikh,[§] Qichao Wu,[†] Jillian M. Buriak,[†] and Tate Hauger[†]

[†]Gunning-Lemieux Chemistry Centre, University of Alberta, 11227 Saskatchewan Drive NW, Edmonton, Alberta, Canada T6G 2G2

[‡]National Research Council Canada, 100 Sussex Drive, Ottawa, Ontario, Canada K1A 0R6

[§]Department of Chemistry, University of Ottawa, 10 Marie Curie Private, Ottawa, Ontario, Canada K1N 6N5

Supporting Information

ABSTRACT: In light of the intense recent interest in the methylammonium lead halides, $CH_3NH_3PbX_3$ (X = Cl, Br, and I) as sensitizers for photovoltaic cells, the dynamics of the methylammonium (MA) cation in these perovskite salts has been reinvestigated as a function of temperature via ^2H, ^{14}N, and ^{207}Pb NMR spectroscopy. In the cubic phase of all three salts, the MA cation undergoes pseudoisotropic tumbling (picosecond time scale). For example, the correlation time, τ_2, for the C−N axis of the iodide salt is 0.85 ± 0.30 ps at 330 K. The dynamics of the MA cation are essentially continuous across the cubic ↔ tetragonal phase transition; however, ^2H and ^{14}N NMR line shapes indicate that subtle ordering of the MA cation occurs in the tetragonal phase. The temperature dependence of the cation ordering is rationalized using a six-site model, with two equivalent sites along the *c*-axis and four equivalent sites either perpendicular or approximately perpendicular to this axis. As the cubic ↔ tetragonal phase transition temperature is approached, the six sites are nearly equally populated. Below the tetragonal ↔ orthorhombic phase transition, ^2H NMR line shapes indicate that the C−N axis is essentially frozen.

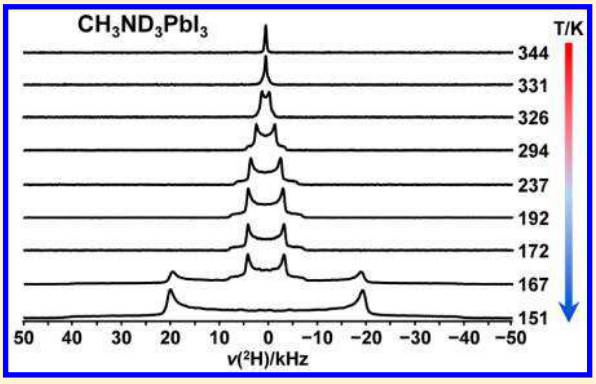

INTRODUCTION

The methylammonium (MA) lead halides $CH_3NH_3PbX_3$ (X = Cl, Br, and I) were first prepared and shown to have a cubic perovskite structure by Weber in 1978.[1] The color of the compounds, cream white (X = Cl), reddish orange (X = Br), and black (X = I), led to the suggestions of a charge-transfer nature of the Pb−X bonds and the possibility of photoconduction.[1,2] These compounds were also of interest because the position of the methylammonium (MA) cation is not fixed by the crystal structure,[3,4] although it is known to reside in a cuboctahedal cage formed by 12 X atoms. In 1985, using ^2H and ^{14}N solid-state NMR spectroscopy, we found evidence that the MA cation in these compounds undergoes rapid effectively isotropic motion in the cubic phases (picosecond time scale).[3] We also identified two lower-temperature phases for the bromide and iodide, and at least one other phase for the chloride. In 1987, Poglitsch and Weber used X-ray diffraction to demonstrate that the lower-temperature phases of these compounds are tetragonal and orthorhombic (Scheme 1).[4] These authors also reported millimeter-wave spectroscopic data that demonstrated picosecond relaxation processes in the cubic and tetragonal phases. Later, we used adiabatic calorimetry to characterize the phase transitions in these three compounds[2] as well as ^2H NMR spectroscopy to confirm that there is an ordering of the MA cations taking place in the tetragonal phase as one cools the sample (Scheme 2). Similar calorimetric data were also reported by Onoda-Yamamuro et al.[5] In 1991, Xu et al.[6] reported the temperature dependence of the ^1H NMR spin−lattice relaxation times for these compounds, as well as ^{35}Cl, ^{81}Br, and ^{127}I nuclear quadrupole resonance (NQR) data.

Using neutron diffraction, Swainson, Knop, and co-workers reported the low-temperature orthorhombic structures of $MAPbBr_3$ in 2003[8] and $MAPbCl_3$ in 2005.[9] Lattice parameters

Scheme 1. Phase Transitions for $MAPbX_3$ Perovskites[2,5]

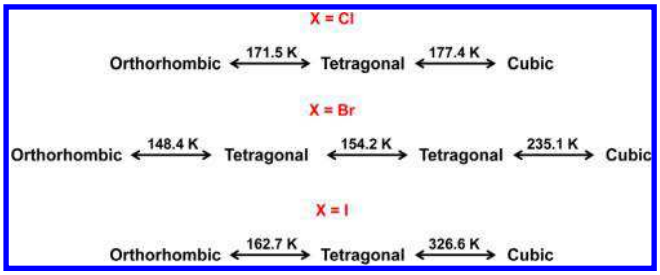

Received: November 23, 2017
Revised: January 9, 2018
Published: January 16, 2018

DOI: 10.1021/acs.jpca.7b11558
J. Phys. Chem. A 2018, 122, 1560−1573

Scheme 2. Asymmetric Units for (A) Orthorhombic, (B) Tetragonal, and (C) Cubic Phases of $MAPbX_3$ Perovskites[a]

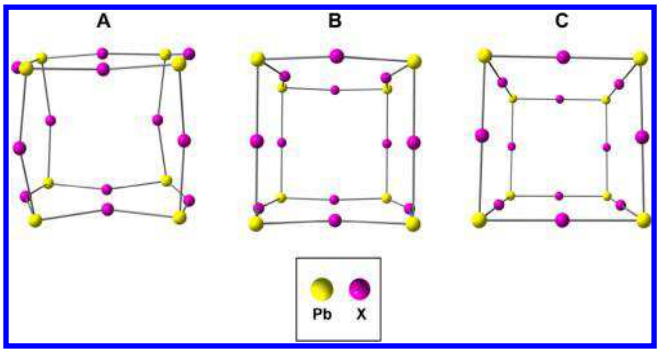

[a]The MA cation, which exhibits dynamic disorder (see text), is not shown. Structures shown here were derived from those reported by Weller et al. for $MAPbI_3$ at 100 (A), 180 (B), and 352 K (C).[7]

for both compounds were determined over a wide temperature range. The changes in structure at the cubic−tetragonal phase transition have also been investigated by Mashiyama et al.[10] The structures of the $MAPbX_3$ compounds have been the subject of several studies;[7−15] for the iodide, we believe that one of the most comprehensive is the neutron powder diffraction data of Weller et al. acquired at 100, 180, and 352 K (Scheme 2).[7] In addition, the recent time-of-flight neutron and synchrotron X-ray powder diffraction study of Whitfield et al. provided important insights.[15] In the orthorhombic phase, the space group is *Pnma*, in the tetragonal phase it is *I*4/*mcm*, and in the cubic phase it is $Pm\bar{3}m$.

Prior to 2009, interest in these compounds was primarily confined to the solid-state-chemistry community,[16] but in that year, Kojima et al. reported that $MAPbI_3$ can be used as a visible-light sensitizer for photovoltaic cells.[17] Although the initial photoconversion efficiency was only a few percent, conversion efficiencies using organometallic lead hybrid perovskites that exceed 20% are currently being reported.[18−24] Charge carrier lifetimes are intimately tied to photovoltaic performance, and for lead halide perovskites, the dynamics of the cation play a key role.[25] Higher rotational momentum of the cation rotor is correlated to better orbital overlap, more facile polaron formation, and thus lower charge carrier recombination and a higher fill factor, leading to higher solar cell efficiencies.[26,27] A complete understanding of the dynamics of these cations within the perovskite materials is critical for improving, in a rational fashion, the optoelectronic performance.[28−31]

The utility of solid-state NMR spectroscopy in the characterization of these materials is illustrated by the numerous recent studies. Baikie et al.[13] used ^{1}H and ^{13}C NMR results to investigate the nature of the MA dynamics in the $MAPbX_3$ compounds which help refine some X-ray and neutron diffraction data on these compounds. Roiland and co-workers[32] undertook a multinuclear magnetic resonance study of these compounds to investigate their local order and dynamics. Kubicki et al.[26] used variable temperature (VT) solid-state NMR to investigate the reorientation dynamics for a series of mixed-cation perovskites; on the basis of ^{2}H and ^{14}N NMR measurements, the authors conclude that the formamidinium cation rotates faster than does the MA cation, despite the greater size of the former. This group also used multinuclear (^{13}C, ^{14}N, ^{39}K, ^{87}Rb, and ^{133}Cs) magnetic resonance to investigate the atomic-level structure of bulk perovskites.[33] Senocrate et al.[34] used multinuclear solid-state magnetic resonance and other experimental techniques including ^{127}I NQR to investigate the behavior of the iodine ions in $CH_3NH_3PbI_3$. Askar and co-workers investigated $MAPbI_3$ and its decomposition products via ^{1}H, ^{13}C, and ^{207}Pb solid-state NMR spectroscopy.[35] Kentgens and co-workers reported results of a VT ^{14}N and ^{207}Pb solid-state NMR and ^{127}I NQR study of $MAPbI_3$. These authors conclude that the MA cation is two-dimensionally disoriented (i.e., restricted to the *ab*-plane) in the tetragonal phase.[36] Rosales et al.[18] used ^{207}Pb NMR spectroscopy to characterize mixed-halide nano- and microcrystalline Pb perovskites. Previously, this research group also used ^{207}Pb NMR spectroscopy to investigate mixed-halide perovskites.[37] Finally, we have recently proposed that the high sensitivity of the ^{207}Pb chemical shifts for $MAPbCl_3$ make this an ideal material for NMR thermometry.[38]

Our goal in this work is to present a comprehensive VT ^{2}H and ^{14}N NMR investigation of the methylammonium lead halide perovskites. NMR line shapes and relaxation data are used to characterize the dynamics of the MA cation in all three $MAPbX_3$ perovskites, with a focus on $MAPbI_3$. For completeness, we also present ^{207}Pb VT NMR data of these perovskites.

NMR BACKGROUND

^{2}H or ^{14}N NMR Line Shapes. The nuclear quadrupolar coupling constant, C_Q, is defined as eQV_{zz}/h, where eQ is the nuclear quadrupole moment of the quadrupolar nucleus and V_{zz} is the largest principal component of the electric field gradient (EFG) tensor. The quadrupolar asymmetry parameter, η_Q, is defined as $(V_{xx} - V_{yy})/V_{zz}$, where $|V_{xx}| \leq |V_{yy}| \leq |V_{zz}|$. Note that the trace of the EFG tensor is zero; i.e., $V_{xx} + V_{yy} + V_{zz} = 0$. For ^{2}H and ^{14}N, both $I = 1$ nuclei, the nuclear quadrupole moments are 2.860 and 20.44 mb, respectively.[39] Figure 1 illustrates the powder pattern expected for such nuclei if $\eta_Q = 0$ (i.e., $V_{xx} = V_{yy}$), in the absence of motion incorporating the observed nucleus. For example, in the absence of motion, $C_Q(^2H)$ values for ^{2}H nuclei within C−D bonds are typically approximately

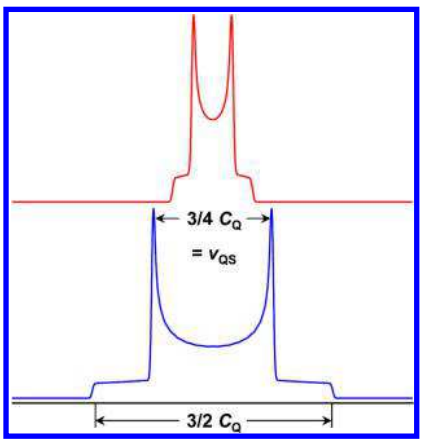

Figure 1. Powder pattern expected for $I = 1$ nuclei with $\eta_Q = 0$. The relationship between C_Q and the breadth of the spectrum illustrated on the lower trace is only observed in the absence of motion. The upper trace illustrates the effect on the spectrum if the nuclei are subject to rapid C_3 jumps about an axis where $\varphi = 109.47°$ (i.e., $\nu_{QS} = (1/4)C_Q$).

DOI: 10.1021/acs.jpca.7b11558
J. Phys. Chem. A 2018, 122, 1560−1573

160 kHz[40] and, with $\eta_Q \approx 0$, the approximate separation between the maxima, ν_{QS}, is 120 kHz.

Significant motion of the nucleus modifies the observed line shape.[41−46] For example, at temperatures slightly below that for the tetragonal ↔ orthorhombic phase transitions, the ^{2}H NMR spectra for the $CH_3ND_3^+$ cation of the three perovskites considered here exhibit axially symmetric powder patterns with ν_{QS} values of approximately 40 kHz. As discussed in our earlier work on these samples[2,3] as well as in an investigation of $CH_3ND_3NO_3$,[47] such a value for ν_{QS} indicates that the C−N axis is restricted to small amplitude wobbling moderated by rapid C_3 jumps of the ND_3 group about the C−N axis. Such motion reduces the observed pattern by a factor $(3\cos^2\varphi - 1)/2$, where φ defines the angle formed by the C−D or N−D bonds with the axis of rotation.[41,45,46] If one assumes that φ = 109.47° (i.e., tetrahedral bonding), then ν_{QS} is reduced by a factor of 1/3, from ≈120 to ≈40 kHz, as illustrated in Figure 1. Significant reduction of ν_{QS} below 40 kHz indicates motion of the C−N axis, which, in favorable cases, may be modeled (vide infra).

NMR Relaxation of Spin *I* = 1 Nuclei. In general, for spin I = 1 quadrupolar nuclei such as ^{2}H or ^{14}N, the main spin−lattice relaxation mechanism is the quadrupolar mechanism

$$R_1^Q = \frac{1}{T_1^Q} = \frac{3}{80}(2\pi C_Q)^2\left(1 + \frac{\eta_Q^2}{3}\right)[J(\omega_0) + 4J(2\omega_0)] \quad (1)$$

where R_1^Q is the rate of relaxation (s^{-1}) via the quadrupolar mechanism and T_1^Q is the spin−lattice relaxation time due to quadrupolar relaxation (note that eq 1 is only valid for nuclei with spin I = 1).[48−52] $J(\omega_0)$ and $J(2\omega_0)$ are spectral densities that are Fourier transforms of autocorrelation functions,[48,49] where

$$J(\omega_0) = \frac{2\tau_c}{1 + \omega_0^2\tau_c^2} \quad (2)$$

In the cubic phases of the three MA lead halides, reorientation of the MA cation is extremely rapid with effective rotational correlation times, τ_c, less than 10^{-9} s (vide infra). Under these conditions $(\omega_0\tau_c)^2 \ll 1$ and $J(\omega_0) = J(2\omega_0) = 2\tau_c$, thus eq 1 reduces to[50−52]

$$R_1^Q = \frac{1}{T_1^Q} = \frac{3}{8}(2\pi C_Q)^2\left(1 + \frac{\eta_Q^2}{3}\right)\tau_c \quad (3)$$

Since, for the ^{2}H and ^{14}N nuclei of the MA cation, $\eta_Q \approx 0$, eq 3 further reduces to

$$R_1^Q = \frac{1}{T_1^Q} = \frac{3}{2}\pi^2 C_Q^2\tau_c \quad (4)$$

In the limit where the molecule is undergoing rotational diffusion, the effective NMR correlation time, $\tau_c = \tau_2$. Note

$$\tau_l = \frac{1}{l(l+1)D} \quad (5)$$

where D is the rotational diffusion constant, and l is the order of the spherical harmonics (for NMR, l = 2; for dielectric relaxation, l = 1), thus $\tau_1 = 3\tau_2$.[53−55] For a prolate symmetric top, such as $CH_3NH_3^+$, the relaxation of the ^{14}N nucleus probes the motion of the C_3 symmetry axis. On the other hand, relaxation of the ^{2}H nuclei depends on both the motion of the C_3 symmetry axis and motion about this symmetry axis.[48,56−58] The relationship between τ_c and the rotational diffusion constants parallel and perpendicular to the C_3 axis, $D_\parallel$ and $D_\perp$, respectively, is given by

$$\tau_c = \frac{(3\cos^2\theta - 1)^2}{24D_\perp} + \frac{3\sin^2\theta\cos^2\theta}{5D_\perp + D_\parallel} + \frac{0.75\sin^4\theta}{2D_\perp + 4D_\parallel} \quad (6)$$

For the ^{14}N nucleus of the methylammonium cation, θ = 0°, $(3\cos^2\theta - 1)^2 = 4$, and thus

$$\tau_c(^{14}\mathrm{N}) = \frac{1}{6D_\perp} \quad (7)$$

If one assumes that the C−N−^{2}H angle is 109.47°, then

$$\tau_c(^2\mathrm{H}) = \frac{1/9}{6D_\perp} + \frac{8/27}{5D_\perp + D_\parallel} + \frac{16/27}{2D_\perp + 4D_\parallel} \quad (8)$$

Clearly, a rotational diffusion model allows one to obtain both $D_\perp$ and $D_\parallel$; however, this is no doubt a rough model, particularly in the tetragonal phase where quadrupolar splittings are observed. Note that the NMR rotational correlation time for ^{14}N is simply τ_2 or $\tau_\perp$.

Critical Phenomena. In solids that exhibit solid−solid phase transitions, the temperature dependence of the physical properties (e.g., lattice parameters, magnetic properties, electric field gradients) can often exhibit critical phenomena.[59] For example, ν_{QS} can be described by an equation of the form

$$\nu_{QS} = a(T_c - T)^n \quad (9)$$

where T_c is the phase transition temperature, a is here expressed in units of kilohertz, and n is the critical exponent.[2,11,15,59,60] Kawamura et al. found that lattice parameters for the tetragonal phase of $MAPbI_3$ are proportional to $(T_c - T)^n$ with n = 0.42.[11]

EXPERIMENTAL SECTION

Deuterium NMR spectra of $MAPbX_3$ or of MAX (X = Cl, Br, I) were obtained at 11.75 T on a Bruker Avance NMR spectrometer and at 21.1 T on a Bruker Avance II NMR spectrometer, operating at 76.8 and 138.1 MHz, respectively. The samples were ^{2}H-enriched at either the carbon or nitrogen of the MA cation. Spectra of the samples in the cubic phase were acquired with single-pulse excitation, while those for samples in the tetragonal or orthorhombic phases were acquired with a solid-echo pulse sequence ($\pi/2-\tau_1-\pi/2-\tau_2-$ACQ, where τ_1 and τ_2, the interpulse and refocusing delays, respectively, were set to 30 to 50 μs and ACQ is the acquisition time); the resulting free induction decays were left shifted to remove points prior to the echo maxima. $\pi/2$ pulses were 5.0 or 8.0 μs for spectra acquired at 11.75 and 21.1 T, respectively. For spectra of the sample in the cubic phase, T_1 relaxation data were obtained with the standard inversion−recovery pulse sequence ($\pi-\tau_{ir}-\pi/2-$ACQ, where τ_{ir} is the variable delay); for the broader NMR powder patterns of the sample in the tetragonal phase, a solid-echo series of pulses was incorporated into the inversion recovery pulse sequence (i.e., $\pi-\tau_{ir}-\pi/2-\tau_1-\pi/2-\tau_2-$ACQ). Recycle delays ranged from 2 s for spectra acquired at lower temperatures (vide infra) to 120 s for those acquired at higher temperatures. Spectra, acquired with ^{1}H decoupling, were referenced to TMS ($\delta(^2\mathrm{H})$ = 0.0 ppm) by setting the ^{2}H peak of $D_2O(l)$ (99.9% ^{2}H) to 4.8 ppm. Samples

DOI: 10.1021/acs.jpca.7b11558
J. Phys. Chem. A 2018, 122, 1560−1573

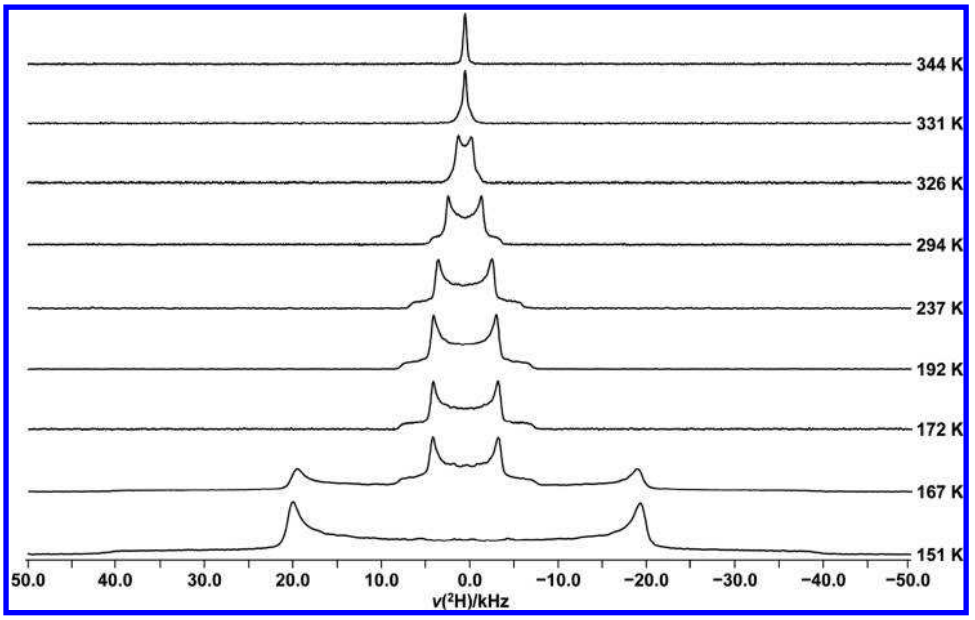

Figure 2. ^{2}H NMR spectra for a stationary sample of $CH_3ND_3PbI_3$, acquired at the indicated temperatures, at 11.75 T.

were packed in 4 mm zirconia rotors; at 11.75 T, a Bruker 4 mm MAS probe was used to acquire the data, while at 21.1 T the rotor was placed into a 5 mm outer diameter glass tube and the spectra were acquired with a Bruker 5 mm H/X solenoid probe.

Nitrogen-14 NMR spectra for the $MAPbX_3$ samples were acquired at 36.1 and 64.5 MHz respectively for spectra acquired at 11.75 and 21.1 T. The $\pi/2$ pulses were 6.0 (11.75 T) or 10.0 μs (21.1 T). Samples were packed in 7 mm outer diameter NMR rotors and acquired with a Bruker 7 mm MAS probe (11.75 T); those acquired at 21.1 T were packed as described above. Recycle delays ranged from 0.25 to 2.0 s, depending on temperature. Spectra, acquired without ^{1}H decoupling, were referenced such that δ_{iso} = 0.0 ppm for an external sample of solid NH_4Cl. ^{14}N spectra for the MAX salts were acquired at 21.1 T with the WURST−QCPMG pulse sequence,[61,62] with a 30 kHz ^{1}H decoupling field and with a 2 s recycle delay; the spikelet spacing was 5.0 kHz. Spectra were acquired in two frequency offset steps and the resulting spectra added to yield the total spectrum.

Lead-207 NMR spectra were obtained with either single pulse excitation or with solid echoes at 4.70 T on a CMX Infinity 200 spectrometer, at 11.75 T on a Bruker Avance spectrometer and at 21.1 T on a Bruker Avance II spectrometer, with 90° pulses ranging from 3.0 to 5.4 μs. Spectra were referenced to the ^{207}Pb chemical shift of $Pb(CH_3)_4$ (δ_{iso} = 0) by setting the isotropic value of a ^{207}Pb NMR spectrum of a stationary sample of $Pb(NO_3)_2$, acquired at 294 K, to −3491.6 ppm. This value is based on that reported by Neue et al. but adjusted for the slightly lower temperature in our lab.[63]

Variable temperature NMR experiments were undertaken at 11.75 and 21.1 T using the Bruker BVT 3000 temperature controller on both instruments. Temperatures were calibrated based on the ^{207}Pb chemical shifts of solid $Pb(NO_3)_2$.[64,65] Dry nitrogen gas, obtained from the boil-off of N_2(liquid), was used as the variable temperature gas. N_2(liquid) was also used for the heat-exchange medium for temperatures below 250 K, while an ethanol/dry ice bath was used in the 250−293 K range.

Relativistic density functional theory (DFT) calculations of the nuclear magnetic shielding and indirect Pb−X spin−spin coupling for model PbX_6 complexes were undertaken with the Amsterdam Density Functional (ADF) program[66−68] mounted on a four-core processor. Relativistic effects were incorporated in the results through the zero-order relativistic approximation (ZORA).[69−72] Octahedral symmetry with $r_{Pb,Cl}$ = 2.85 Å, $r_{Pb,Br}$ = 2.98 Å, and $r_{Pb,I}$ = 3.20 Å was used for the calculations, undertaken with a triple-ξ basis set incorporating two polarization functions (TZ2P) and a quadruple-ξ basis set incorporating four polarization functions (QZ4P). Calculated magnetic shielding was converted to chemical shift according to $\delta(^{207}Pb)_{calc} = \sigma(Pb)_{ref} - \sigma(Pb)_{calc}$, where $\sigma(Pb)_{ref}$ is the magnetic shielding for the reference compound, $Pb(CH_3)_4$, calculated at the same level of theory. The structure for $Pb(CH_3)_4$ was that reported by Oyamada et al.[73]

Lead(II) acetate trihydrate (ACS grade) and lead(II) dichloride were purchased from Fisher Scientific. HCl (37% in H_2O) was purchased from Caledon Laboratories, while HBr (48% in H_2O), HI (57% in H_2O), and methylamine (40% in H_2O) were purchased from Sigma-Aldrich. Methyl-d_3-amine HCl (99.5% ^{2}H) and D_2O (99.9% ^{2}H) were purchased from MSD Isotopes, Montreal.

$MAPbX_3$ compounds were synthesized as per the procedures described in refs 1 and 2. The deuterated versions were prepared according to the procedures described in refs 2 and 9. X-ray diffraction (XRD) spectra were collected on a Bruker AXS D8 diffractometer with a large-area detector using a Cu Kα radiation source.

RESULTS AND DISCUSSION

The tetragonal and orthorhombic phases of the $MAPbX_3$ salts are in effect distortions of the cubic phase, and in all three phases it is reasonable to consider that the MA cation is located inside a pseudocube, where the eight corners are the Pb atoms with the 12 edges consisting of linear or bent halogen atom bridges between two Pb atoms (Scheme 2). In the orthorhombic phase for $MAPbI_3$ determined by powder neutron diffraction,[7,14,15] the C−N axis of the MA cation is

DOI: 10.1021/acs.jpca.7b11558
J. Phys. Chem. A 2018, 122, 1560−1573

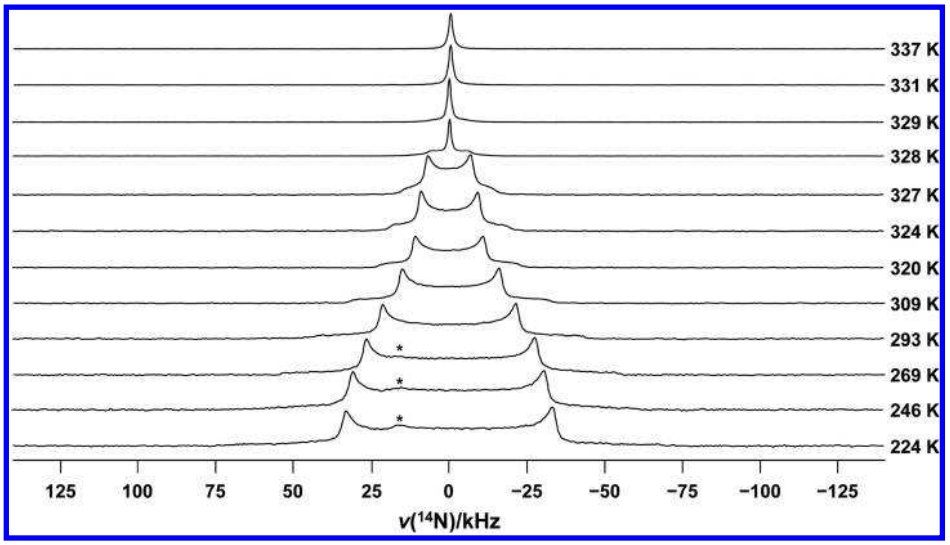

Figure 3. ^{14}N NMR spectra of a stationary sample of $CH_3NH_3PbI_3$, acquired at 21.1 T at the indicated temperatures. The asterisks indicate ^{14}N signal from the VT gas, N_2.

fixed in the plane perpendicular to the long axis of the unit cell and points toward a face of the pseudocube. Similarly, the neutron diffraction data acquired at 180 K suggests that in the tetragonal phase the C−N axis is also close to the plane perpendicular to the long axis of the unit cell, but disordered over four equivalent positions, and although tilted slightly out of the plane, the C−N axis still points toward the pseudocube faces.[7] In a neutron diffraction study of the isostructural tetragonal phase of the $MAPbBr_3$ salt,[8] it was also suggested that the data supported orientational disorder of MA cations in this plane. An X-ray diffraction study[11] of $MAPbI_3$ also suggested four disordered positions of the C−N axis, albeit tilted further out of the plane perpendicular to the *c*-axis. Similarly, Mashiyama and co-workers,[10] Baikie et al.,[13] and Yin et al.[74] have investigated the structure of the higher-temperature tetragonal phase of $MAPbBr_3$.

Figure 2 illustrates ^2H NMR spectra for $CH_3ND_3PbI_3$, acquired at 11.75 T in the 151−344 K range. The spectrum acquired at 151 K consists of an axially symmetric powder pattern with a ν_{QS} value of 40 kHz, approximately 1/3 the value expected in the absence of motion of the MA cation.[40] These results are consistent with the determined structure, indicating that the only significant motion is the rapid reorientation of the ND_3 group about the C−N axis. The spectrum acquired at 167 K illustrates the abrupt change in dynamics of the MA cation at the tetragonal ↔ orthorhombic phase transition. The axially symmetric powder pattern with ν_{QS} = 38.9 kHz is due to crystallites in the orthorhombic phase, while the narrower pattern, ν_{QS} = 7.8 kHz, is due to crystallites that are in the tetragonal phase. Values of ν_{QS} decrease as the temperature is increased, such that $\nu_{QS} \sim 1.7$ kHz at 326 K. A plot of ν_{QS} vs $1000/T$ for $CH_3ND_3PbI_3$ is shown in Figure S1 of the Supporting Information. Likewise, for the $CD_3NH_3^+$ cation of $MAPbI_3$, ν_{QS} decreases from ~7.0 kHz at 198 K to ~1.8 kHz at 325 K, as shown in Figure S2. At temperatures greater than the tetragonal ↔ cubic phase transition (i.e., >326.6 K), ν_{QS} = 0 for both $CH_3ND_3PbI_3$ and $CD_3NH_3PbI_3$; Figure S3 shows that the temperature dependence of $\nu_{QS}(^2H)$ is virtually identical for these two isotopomers.

Figure 3 illustrates a series of ^{14}N NMR spectra of $MAPbI_3$ acquired at various temperatures. ^{14}N ν_{QS} values for the salt in the tetragonal phase range from 76.5 kHz at 175 K to 14.4 kHz at 327 K. There is no indication of magnetic shielding anisotropy in these spectra. Unfortunately it was not possible to obtain ^{14}N NMR spectra for the salt in the orthorhombic phase, so the ν_{QS} value in the absence of significant motion of the C−N bond axis has been estimated (vide infra). The ^{14}N NMR line shapes are consistent with axially symmetric EFG tensors in the fast motion limit (i.e., they do not show the distortions observed for an activated motion in the intermediate rate regime).[41−43] The splittings observed for the tetragonal phase rapidly decrease as the temperature approaches the tetragonal ↔ cubic phase transition temperature, and can be fit to an equation with a critical-temperature dependence (Figure 4). As

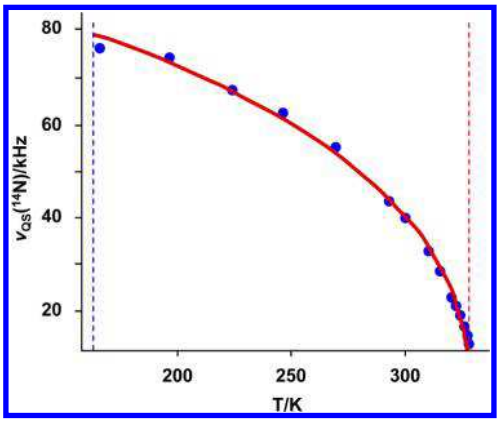

Figure 4. Plot of $\nu_{QS}(^{14}N)$ vs T for $MAPbI_3$, which was fit to eq 9 with a = 11.39 kHz and n = 0.3813, R^2 = 0.9878. The cubic ↔ tetragonal and tetragonal ↔ orthorhombic phase transition temperatures are indicated with red and blue dashed lines, respectively.

for the ^2H spectra discussed above, at the transition to the cubic phase the ^{14}N quadrupolar powder pattern collapses, leaving a symmetric Gaussian peak, consistent with rapid pseudoisotropic reorientation of the C−N axis in the cubic lattice.

Estimating $C_Q(^{14}N)$ from ^2H and ^{14}N NMR Line Shapes. As discussed below, determination of rotational correlation times for the MA cation requires knowledge of the ^2H and ^{14}N C_Q values. These values must not be reduced by motional

DOI: 10.1021/acs.jpca.7b11558
J. Phys. Chem. A 2018, 122, 1560−1573

Table 1. Order Parameters and Calculated ν_{QS} Values for $MAPbBr_3$ and $MAPbI_3$

salt	nucleus	T_c/K	T/K	a/kHz	n	ν_{QS}[a]/kHz	R^2
$CH_3ND_3PbI_3$	^{14}N	326.6	162.7	11.39	0.3813	79.6	0.9878
$CH_3ND_3PbI_3$	^{2}H	326.6	162.7	1.270	0.357	7.9	0.9889
$CD_3NH_3PbI_3$	^{2}H	326.6	162.7	1.129	0.374	7.6	0.9843
$CH_3ND_3PbBr_3$	^{14}N	235.1	148.4	6.497	0.431	43.2	0.9958
$CH_3ND_3PbBr_3$	^{2}H	235.1	148.4	0.3438	0.5611	4.0	0.9720

[a]Expected ν_{QS} values immediately above the tetragonal ↔ orthorhombic phase transition temperature, derived from best fits to eq 9.

averaging and, in principle, should be determined for the sample in the same environment (i.e., the tetragonal phase in this case) for which the correlation times are being measured. Of course this is not practical for the $MAPbX_3$ salts, since the MA cation is known to be undergoing rapid motion above the tetragonal ↔ orthorhombic phase transition,[3] so, for ^2H, this value will be derived from the $\nu_{QS}(^2H)$ value measured for the sample in the orthorhombic phase. Unfortunately, hardware limitations precluded direct measurement of $\nu_{QS}(^{14}N)$ for $MAPbI_3$ in the orthorhombic phase (vide infra), so $C_Q(^{14}N)$ was estimated according to

$$C_Q(^{14}N) = \frac{4}{3}\frac{\nu_{QS}(^2H)_{ortho}}{\nu_{QS}(^2H)_{max,tetra}}\nu_{QS}(^{14}N)_{max,tetra} \quad (10)$$

where $\nu_{QS}(^2H)_{ortho}$ is the $\nu(^2H)$ value for the sample in the orthorhombic phase and "max,tetra" indicates the maximum quadrupolar splitting in the tetragonal phase for the indicated nucleus. For $CH_3ND_3PbI_3$, the maximum ^2H ν_{QS} values that we observed in the orthorhombic and tetragonal phases are 40.0 and 7.9 kHz, respectively. Since the ^2H and ^{14}N ν_{QS} values appear to vary with temperature in a fashion analogous to the lattice parameters, $\nu_{QS}(^{14}N)$ at the tetragonal ↔ orthorhombic phase transition temperature may be estimated from the order parameters a and n obtained from a fit of $\nu_{QS}(^{14}N)$ vs T to eq 9 (see Figure 4 for the fit for the $MAPbI_3$ data); the order parameters resulting from these fits and the ν_{QS} values expected at the tetragonal ↔ orthorhombic phase transition temperature are listed in Table 1. For $MAPbI_3$, $\nu_{QS}(^{14}N)_{max,tetra} \approx 80$ kHz at this temperature and thus, from eq 10, $C_Q(^{14}N)$ values of 525–540 kHz are predicted, depending on whether $\nu_{QS}(^2H)$ values for the $CD_3NH_3^+$ or $CH_3ND_3^+$ isotopomers are considered. Acknowledging that the C–N axis may be undergoing some small amplitude wobbling in the high-temperature region of the orthorhombic phase (i.e., at 151.3 K), our value for $\nu_{QS}(^2H)_{ortho}$ for a rigid C–N axis, 40 kHz, may be 2 or 3 kHz lower than the value expected in the absence of any motion. For example, a maximum ^2H splitting of 42 kHz yields $C_Q(^{14}N) = 570$ kHz. In the calculations that follow we will use $C_Q(^{14}N) = 550 \pm 80$ kHz. Our estimated value is within experimental error of the value calculated by Kentgens and co-workers (600 kHz)[36] but smaller than the calculated value reported by Kubicki et al. (770 kHz).[26]

We also examined the temperature dependence of $\nu_{QS}(^2H)$ and $\nu_{QS}(^{14}N)$ for $MAPbBr_3$; see Table 1 as well as Figures S4 and S5 in Supporting Information. At the tetragonal ↔ orthorhombic phase transition for the bromide, $\nu_{QS}(^2H)$ and $\nu_{QS}(^{14}N)$ values of 4.0 and 43 kHz are expected, based on the order parameters summarized in Table 1. Both these values are approximately half the corresponding values for the iodide, indicating greater disorder of the MA cation in the bromide (vide infra). Also, our value of $\nu_{QS}(^2H)$ in the orthorhombic phase is in excellent agreement with the value measured at 50 K by Roiland et al.[32] Using eq 10 and the data summarized in Table 1, $C_Q(^{14}N)$ for $MAPbBr_3$ is approximately 570 kHz, again probably a lower limit.

The narrow range of temperatures for which $MAPbCl_3$ exists in the tetragonal phase precluded a similar treatment for this salt. Reported values of $C_Q(^{14}N)$ for an MA cation that is assumed to be stationary range from 413 kHz for MA perchlorate[75] to 959 ± 3.0 kHz in MA chloride.[76] We have also obtained ^{14}N (Figure S6) and ^2H (Figure S7) NMR data for the methylammonium halides; Table S1 summarizes the data for these samples obtained at several temperatures. At 293 K, all three salts are in the tetragonal phase, $P4/nmm$, where motion of the CH_3 and NH_3 groups are confined to rotations about the C–N bond. $C_Q(^{14}N)$ values for the MAX salts decrease on going from X = Cl to X = I (960, 895, and 785 kHz for data measured at 293 K). In contrast, the corresponding $\nu_{QS}(^2H)$ values increase slightly: 34.1 (X = Cl), 37.9 (X = Br), and 39.2 kHz (X = I).

Modeling the Disorder of the MA Cation in the Tetragonal Phase for $CH_3ND_3PbI_3$. The ^2H line shapes for the MA cation (e.g., see Figure 2), with an asymmetry parameter $\eta = 0$, are consistent with rapid reorientation about an n-fold axis with $n > 2$. As discussed above, the ^2H NMR spectra acquired for the $MAPbX_3$ salts below the tetragonal ↔ orthorhombic phase transition temperature indicate rapid reorientation about the C–N axis, yielding an averaged, axially symmetric quadrupole coupling tensor with its unique component along the C–N axis. Any further averaging (i.e., a further reduction of ν_{QS}) reflects reorientation of the C–N axis itself. The structure refinement with space group $I4cm$[12] puts the C–N axis parallel to the c-axis, in which case there can be no further narrowing of the NMR line shape, from $\nu_{QS}(^2H) = 40$ kHz, in the tetragonal phase; thus the ^2H and ^{14}N results rule out this structural model. Most of the refinements,[7,8,11,14,15] including the two most recent,[14,15] assign the tetragonal phase to space group $I4/mmm$, in which the C–N axis must be disordered over four or eight positions, depending on the model, to conform to the symmetry. Dynamic disorder will lead to narrowing of the ^2H and ^{14}N line shapes. If reorientation of the C–N axis is restricted to the four orientations determined in these refinements, one obtains averaged ^2H NMR line shapes with quadrupolar splittings that in all but one case (ref 15) do not match observations: since the quadrupolar tensor is insensitive to inversion, the averaging over the four orientations can be modeled as a C_4 rotation. For simple 4-fold rotation when the initial EFG tensor has $\eta = 0$, the averaging equations reduce to

$$\nu_{QS} = V\frac{3\cos^2\beta - 1}{2} \quad (11)$$

where V is the initial quadrupolar splitting (i.e., the splitting expected in the absence of motion of the C–N bond), assumed

DOI: 10.1021/acs.jpca.7b11558
J. Phys. Chem. A 2018, 122, 1560–1573

Table 2. Calculated Populations Based on $\nu_{QS}(^2H)$ Values for the Six-Site Model

$\nu_{QS}(^2H)$[a]/kHz	4 sites[b]/% β = 90°	2 sites[b]/% β = 0°	4 sites[b]/% β = 77.7°	2 sites[b]/% β = 0°	4 sites[b]/% β = 56.6°	2 sites[b]/% β = 0°
0.0	66.67	33.33	69.84	30.16	95.65	4.35
1.0	68.33	31.67	71.58	28.42	98.04	1.96
2.0	70.00	30.00	73.33	26.67	100.43	−0.43
3.0	71.67	28.33	75.07	24.93	102.83	−2.83
4.0	73.33	26.67	76.82	23.18	105.22	−5.22
5.0	75.00	25.00	78.57	21.43	107.61	−7.61
6.0	76.67	23.33	80.31	19.69	110.00	−10.00
7.0	78.33	21.67	82.06	17.94	112.39	−12.39
8.0	80.00	20.00	83.80	16.20	114.78	−14.78
9.0	83.33	16.67	85.55	14.45	117.17	−17.17
10.0	83.42	16.58	87.29	12.71	119.57	−19.57

[a]Expected $\nu_{QS}(^2H)$ value for V = 40.0 kHz. ν_{QS} and V are assumed to have opposite signs. [b]The total population for the four or two sites of an orientation type is listed.

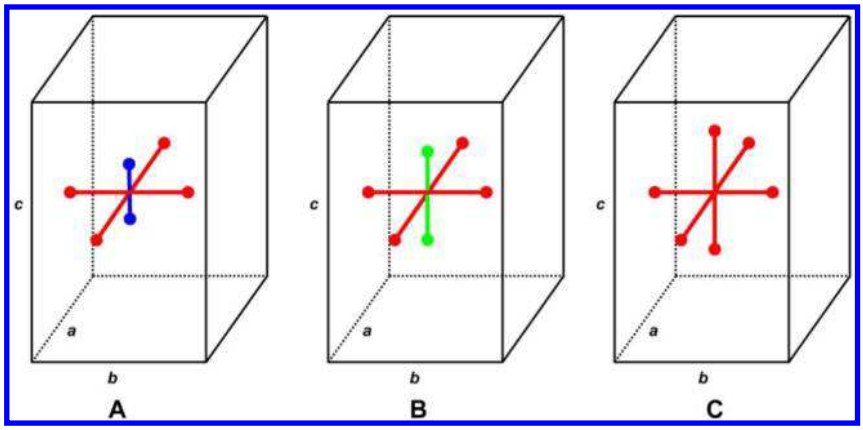

Figure 5. Representation of the population distribution of the MA cation for $MAPbI_3$ with β = 90° in the tetragonal phase near the tetragonal ↔ orthorhombic phase transition temperature (A), in the tetragonal phase near the tetragonal ↔ cubic phase transition temperature (B), and when the sample is in the cubic phase (C). Note that (A) and (B) represent asymmetric units rather than the unit cell, and that edges are not drawn to scale: $a = b \neq c$ for (A) and (B), and $a = b = c$ for (C).

to be 40.0 kHz, the splitting measured at 151 K for X = I, and β is the angle between the C−N axis and the c direction of the crystal. Note that, for an angle of β = 54.736°, the calculated splitting would be zero.

Based on the available C and N atomic coordinate data from each of the four *I*4/*mmm* refinements, we calculated the orientation of the C−N bond relative to the crystal c-axis to obtain the β value and then determined the expected averaged $\nu_{QS}(^2H)$ value for a four-site model: for the neutron powder diffraction structure determined by Weller et al. at 180 K,[7] β = 77.7° and a $\nu_{QS}(^2H)$ value of 17.3 kHz is predicted with this model, significantly greater than the observed value of 7.5 kHz at 180 K. Similarly, based on the single-crystal X-ray structure of Kawamura et al. obtained at 220 K,[11] β = 56.6° and a $\nu_{QS}(^2H)$ value of 1.82 kHz is predicted, significantly less than the value of 6.7 kHz observed at this temperature. For the recent single crystal neutron diffraction structure by Ren et al. at 295 K,[14] β = 66.05° giving an expected $\nu_{QS}(^2H)$ value of 10.112 kHz, compared to an observed value of 4.0 kHz measured at 294 K, and for the neutron powder and synchrotron X-ray diffraction structure reported by Whitfield et al. at 190 K,[15] β = 62.23° yielding an expected $\nu_{QS}(^2H)$ value of 6.973 kHz, compared to an observed value of 7.4 kHz at 192.4 K. Only in the last case is there any reasonable agreement, and considering that correct refinement of disordered structures can be fraught with difficulty, as noted by the authors,[15] even that agreement may be accidental.

The foregoing discussion demonstrates that a simple four-site model of the disorder in the structural refinement is not adequate. However, the introduction of another two equivalent sites along the c-axis (C−N up and down) with a lower population than the original four sites will yield a modified ν_{QS}. With the total population normalized to 1.0 and the four equivalent sites each with a population x, then the sum of the latter is $4x$ and the two equivalent c-axis sites each have a population $(1 - 4x)/2$. The averaging equation becomes

$$\nu_{QS} = V\left[4x\frac{3\cos^2\beta - 1}{2} + \left\{2\left(\frac{1-4x}{2}\right)\right\}\frac{3\cos^2 0 - 1}{2}\right]$$
$$= V[1 - 6x(1 - \cos^2\beta)] \quad (12)$$

In the very symmetric case where all the orientations are orthogonal, i.e., β = 90°, then

$$\nu_{QS} = V[1 - 6x] \quad (13)$$

The choice of this simple six-site model is based on known information: First, diffraction studies of samples in both the orthorhombic and tetragonal phases indicate that the C−N axis is preferentially aligned toward the faces of the pseudocube, angled close to the plane perpendicular to the c-axis.[7,11,14,15] Second, recent molecular dynamics (MD) calculations also suggest a greater preference for orientations of the C−N axis toward the faces of the pseudocube, both from a classical MD

DOI: 10.1021/acs.jpca.7b11558
J. Phys. Chem. A 2018, 122, 1560−1573

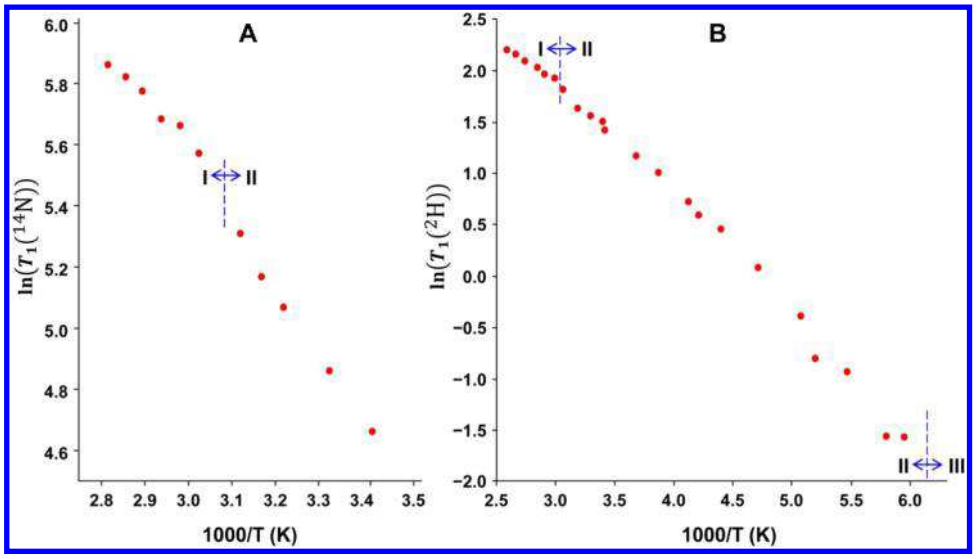

Figure 6. $\ln(T_1)$ plotted as a function of $1000/T$ (K) for the ^{14}N (A) and ^{2}H (B) spin−lattice relaxation of $CH_3NH_3PbI_3$ and $CH_3ND_3PbI_3$, respectively. From the ^{14}N data, $E_A = 11.3 \pm 2$ kJ·mol^{-1} for the salt in the cubic phase (first six points) and 18.1 kJ·mol^{-1} when in the tetragonal phase (last five points). Likewise, from the ^{2}H data, $E_A = 5.9 \pm 1$ kJ·mol^{-1} for the salt in the cubic phase and 7.9 ± 2 kJ·mol^{-1} if the first six points for the salt in the tetragonal phase are considered, or 10.0 ± 2 kJ·mol^{-1} if all points are considered.

investigation by Mattoni et al.[77] and from quantum MD studies[78,79] (see also Figure 4c of ref 80). The classical MD simulations were done as a function of temperature and suggest that in the tetragonal phase there is a greater preference for C−N orientations in the *ab*-plane facing toward the pseudocube faces, but that as the temperature increased there are an increasing number of orientations aligned with the *c*-axis. Furthermore, sites with inequivalent populations imply an energy difference, and the thermal population of the higher energy sites increase relative to the lower energy sites as the temperature increases, thus causing ν_{QS} to decrease. However, for all sites and their populations to become equivalent at the transition to the cubic phase, the energy difference must decrease to zero so that all sites become equivalent at the transition. This is clearly linked to the known tilting of the corner-sharing PbI_6 octahedra in the tetragonal phase.[81]

Table 2 lists populations for the two types of sites calculated for the $-ND_3$ group from this six-site model, for ν_{QS} values ranging from 0 to 10 kHz, and assuming a splitting of 40.0 kHz before dynamic averaging due to motion of the C−N bond. Note that only for $\beta = 90°$ do the populations become equal when $\nu_{QS} = 0$. When β is set to the approximate value reported from the neutron diffraction study,[7] 77.7°, the relative populations are generally reasonable, although they do not reach equal populations for $\nu_{QS} = 0$, but for the β value from the X-ray diffraction study,[11] 56.6°, unreasonable or impossible populations are obtained. Note that it is quite conceivable that, in the tetragonal phase, β is indeed less than 90°, and that with increasing temperature β tends toward 90°. See Figure 5 for a representation of this model where $\beta = 90°$.

For the value of $\nu_{QS} = 7.5$ kHz determined at 180 K, we calculate that the two on-axis sites account for only 20.8% ($\beta = 90°$) or 17.1% ($\beta = 77.7°$) of the total population. Thus, the small on-axis population may have gone unnoticed in the structure refinement. These observations prompt the question: could existing or future diffraction data on $MAPbI_3$ be refined with the suggested six-site model, and would such analyses yield reasonable or even improved *R* factors? Other models can be considered, including eight sites with C−N oriented in the directions of the corners of the pseudocube, or 12 sites oriented toward the edges of the pseudocube, but neither of these is consistent with observations from diffraction studies. The ab initio quantum MD simulations reported by Leguy et al.[80] also show that the corners are the least favored orientations, with slightly more alignment density along the edges, and the greatest alignment toward the faces.

For the methylammonium lead bromide, $MAPbBr_3$, this same model is probably valid, since the tetragonal phase II (i.e., the higher-temperature phase of the two tetragonal phases for $MAPbBr_3$) is in space group *I*4/*mmm* and is probably isostructural with tetragonal $MAPbI_3$.[8] With $\nu_{QS}(^2H) \approx 4.0$ kHz at 163 K, a population of roughly 27% for the two sites (i.e., those parallel to *c*) is calculated, compared to approximately 20% for the iodide at this temperature (see Table 2).

Dynamics of the MA Cation for $MAPbI_3$. Figure 6 illustrates a plot of $\ln(T_1)$ vs $1000/T$ for the ^{14}N and ^{2}H data for $MAPbI_3$; similar plots for ^{2}H data acquired for the Br and Cl salts are illustrated in Figures S8 and S9. Table 3 summarizes ^{14}N and ^{2}H T_1 relaxation data obtained for $MAPbI_3$, as well as correlation times derived from that data. The determination of correlation times at a given temperature as outlined below requires the determination of $T_1(^2H)$ and $T_1(^{14}N)$ values at that temperature, but in some cases, the former were not obtained at the same temperatures as for the ^{14}N data. In such cases, ^{2}H values were obtained by interpolation based on fits of the measured $T_1(^2H)$ (see Figure 6). Here we will focus on rotational correlation times for the MA cation of $MAPbI_3$; however, rotational correlation times from ^{2}H NMR relaxation data for all three halides will be summarized. First, it is important to recognize that NMR measures τ_2 while dielectric relaxation measures τ_1 and, in the special case of rotational diffusion, $\tau_1 = 3\tau_2$.[82]

The dynamics of the MA cation were first investigated by us in 1985.[3] At 303 K, ^{2}H T_1 data lead to rotational times, τ_c, of approximately 0.35 ps for X = Cl and Br, and 0.46 ps for the iodide. Note that the iodide is in the tetragonal phase at this temperature while the chloride and bromide are in the cubic

DOI: 10.1021/acs.jpca.7b11558
J. Phys. Chem. A 2018, 122, 1560−1573

Table 3. ^{14}N and ^{2}H Spin−Lattice Relaxation Data for $MAPbI_3$[a]

T/K	$T_1(^{14}N)$/s	$\tau_\perp(^{14}N)$/ps	$T_1(^{2}H)$/s	$\tau_c(^{2}H)$/ps	$\tau_\parallel$[b]/ps	$\tau_\perp/\tau_\parallel$
			Cubic			
355	0.354	0.632	7.71	0.342	0.180	3.5
350	0.339	0.659	7.47	0.353	0.184	3.6
345	0.324	0.689	7.23	0.365	0.187	3.7
340	0.296	0.755	7.00	0.377	0.183	4.1
335	0.289	0.772	6.76	0.39	0.192	4.0
330	0.264	0.846	6.53	0.404	0.189	4.5
			Tetragonal			
320	0.203	1.10	5.58	0.473	0.201	5.5
315	0.176	1.27	5.32	0.496	0.193	6.6
310	0.159	1.40	5.07	0.52	0.193	7.2
300	0.129	1.73	4.58	0.576	0.194	8.9
293	0.106	2.11	4.25	0.621	0.185	11.4

[a]^{2}H data are for the $CH_3ND_3PbI_3$ isotopomer. [b]$\tau_\parallel = (6D_\parallel)^{-1}$. $\tau_\parallel$ values were obtained from $\tau_\perp$ values and $\tau_c(^{2}H)$ using eq 8.

phase. Rotational correlation times were derived from ^{14}N T_1 data at 303 K for X = Cl and Br using an early $C_Q(^{14}N)$ obtained from liquid crystal data, 1.107 MHz;[83] these analyses yielded τ_2 values of approximately 0.22 and 0.24 ps, respectively. A similar value of τ_2, 0.2 ps, was obtained for the iodide at 333 K, just above the tetragonal ↔ cubic phase transition temperature, 326.6 K. Now we know that it is unlikely that $C_Q(^{14}N)$ in the iodide exceeds 700 kHz, so this would increase the value of τ_2 by a factor of $(1.107/0.700)^2$, a factor of 2.5, i.e., τ_2 = 0.5 ps. Unfortunately, hardware limitations combined with the nuclear properties of ^{14}N (relatively low Larmor frequency and a large quadrupole moment) rendered impractical the acquisition of ^{14}N NMR spectra for the $MAPbX_3$ perovskites in their orthorhombic phase. Our data point toward $C_Q(^{14}N)$ = 550 ± 80 kHz; had this value been used in our early paper,[3] the reported correlation time at 333 K would have been greater by a factor of 4.05 and $\tau_2 \approx 0.8$ ps, in good agreement with our present data; see Table 3.

Poglitsch and Weber used dielectric measurements to determine rotational correlation times at 300 K.[4] For $MAPbX_3$, τ_1 values of 5.63, 2.73, and 5.37 ps were obtained for the chloride, bromide, and iodide, respectively. These values are longer than our values as expected given that $\tau_1 \approx 3\tau_2$ in the limit of rotational diffusion; however, the agreement is only approximate. For a recent review of correlation times and activation energies for $MAPbI_3$, see Mattoni et al.[84]

The correlation time, τ_c, for a cation such as MA^+ is comprised of components that are perpendicular and parallel to the molecular C−N axis, $\tau_\perp$ and $\tau_\parallel$, respectively, as shown in Figure 7. However, since the ^{14}N relaxation of this cation depends only on motion of the C−N bond, $\tau_c(^{14}N) = \tau_\perp(^{14}N)$.

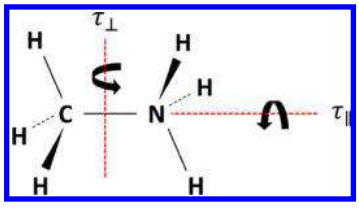

Figure 7. Perpendicular ($\tau_\perp$) and parallel ($\tau_\parallel$) components of τ_c for the MA cation.

The latter was calculated from eq 4, the ^{14}N T_1 data, and the estimated value for $C_Q(^{14}N)$, 550 kHz. Likewise, $\tau_c(^{2}H)$ was calculated from the corresponding ^{2}H data and $C_Q(^{2}H) \approx 160$ kHz. $D_\perp$ was determined from eq 7 and the value for $\tau_\perp(^{14}N)$. Finally, from this value and the value for $\tau_c(^{2}H)$, and eq 8, $D_\parallel$ and $\tau_\parallel$ were calculated. Note that $\tau_\parallel$ shows little variation with temperature (i.e., the rate of rotation of the ND_3 group about the C−N axis exhibits little variation with temperature). In contrast, the motion of the C−N axis is strongly dependent on temperature. Clearly the motion becomes more anisotropic with decreasing temperature. It is recognized that a simple rotational diffusion model is not strictly valid for the MA cation of $MAPbI_3$, particularly in the tetragonal phase, but the results are believed to be qualitatively valid.

It is important to emphasize that both the ^{2}H and ^{14}N T_1 values for $MAPbI_3$ are essentially continuous across the cubic to tetragonal phase. For example, at 330 K (cubic phase) the ^{14}N and ^{2}H values are 0.264 ± 0.013 and 6.53 ± 0.33 s, while at 320 K (tetragonal phase) these values are 0.203 ± 0.010 and 5.58 ± 0.28 s, respectively. Obviously the T_1 values decrease slightly because the temperature has decreased by 10 K, but clearly the change in dynamics across the phase transition is subtle. Similar ^{14}N relaxation data for $MAPbI_3$ were recently reported by Senocrate et al.;[34] plots of ln $T_1(^{14}N)$ vs T^{-1} yielded E_A values of 0.1 eV (9.6 kJ·mol^{-1}) and 0.16 eV (15.4 kJ·mol^{-1}), within experimental error of the values we obtained (Table 4). Also,

Table 4. Apparent Activation Energies for the $MAPbX_3$ (X = Cl, Br, I) Perovskites Derived from ^{2}H and ^{14}N T_1 Data[a]

perovskite	nucleus	phase	E_A/kJ·mol^{-1}	T/K
$CD_3NH_3PbCl_3$	^{2}H	cubic	6.3(1.4)	178−353
$CH_3ND_3PbCl_3$	^{2}H	cubic	5.7(1.1)	188−373
$CH_3ND_3PbCl_3$	^{14}N	cubic	9.2(1.8)	183−313
$CH_3ND_3PbBr_3$	^{2}H	cubic	5.4(1.1)	238−313
$CH_3ND_3PbBr_3$	^{2}H	tetragonal	9.8(2.0)	227−183
$CH_3ND_3PbBr_3$	^{14}N	cubic	9.4(2.0)	243−353
$CH_3ND_3PbI_3$	^{2}H	cubic	5.9(1.0)	334−385
$CH_3ND_3PbI_3$	^{2}H	tetragonal	7.9(2.0)	258−313
$CH_3ND_3PbI_3$	^{14}N	cubic	11.3(2.0)	330−355
$CH_3ND_3PbI_3$	^{14}N	tetragonal	18.1(2.0)	294−320

[a]E_A values are apparent energies over the indicated temperature ranges. The plots of ln(T_1) vs 1000/T exhibit non-Arrhenius behavior. In such cases the E_a values were derived from the initial slopes near the tetragonal ↔ cubic phase transition. For example, ^{2}H T_1 data for $CH_3ND_3PbI_3$ yield $E_A \approx 10$ kJ·mol^{-1} if all data in the tetragonal phase are considered. See the captions to Figure 6 and Figures S8 and S9 for more details.

Baikie et al.[13] found proton T_1 values to be essentially continuous across the cubic to tetragonal phase transition, again confirming little change in the rotational correlation time at the phase transition. For $MAPbBr_3$, we also find the ^{2}H T_1 values to be continuous across the cubic to tetragonal phase transition: 3.46 ± 0.17 s at 238 K and 2.79 ± 0.14 s at 227 K (see Figure S8).

Interpretation of the ^{14}N T_1 data in the cubic phases of the $MAPbX_3$ salts is unambiguous (see eq 3). Given that the ^{1}H, ^{2}H, and ^{14}N T_1 values are essentially continuous across the cubic ↔ tetragonal phase transition, we believe that the rotational correlation times of the MA cation are also continuous to a first approximation. Obviously the observation of a small quadrupolar splitting as one enters the tetragonal

DOI: 10.1021/acs.jpca.7b11558
J. Phys. Chem. A 2018, 122, 1560−1573

Table 5. ^{207}Pb NMR Data for $MAPbX_3$ in the Cubic Phase[a]

		X = Cl	X = Br	X = I
δ_{iso}/ppm	expt	−646(1)	354(5)	1482(10)[b]
	Calc1[c]	−1162	−236	489
	Calc2[c]	−892	204	1455
$\nu_{1/2}$/kHz; 4.70 T	expt	3.6(2)	–	–
$\nu_{1/2}$/kHz; 7.05 T	expt	3.1(2)	16(1)	–
$\nu_{1/2}$/kHz; 11.75 T	expt	3.3(2)	15(2)	21(2)[d]
$\nu_{1/2}$/kHz; 21.14 T	expt	3.7(2)[e]	16(1)	22(2)[b]
$^1J(^{207}Pb,X)$/Hz	expt	400(40)	–	–
	Calc1[c]	460	2128	2166
	Calc2[c]	644	3207	3075
$^1K(Pb,X)_{obs}/10^{20}$ N·A^{-2} m^{-3}	expt	168(17)	–	–
	Calc1[c]	185.8	311.3	426.7
	Calc2[c]	260.2	469.1	605.8

[a]Measured on nonspinning samples at 293 K unless otherwise specified; spectra were acquired either with a Hahn echo or with single-pulse excitation. $\nu_{1/2}$ = full width at half-maximum. [b]Measured at 335 K. [c]Calc1, TZ2P basis set; Calc2, QZ4P basis set. Calculated magnetic shielding was converted to chemical shifts based on the corresponding lead magnetic shielding of $PbMe_4$: σ(Pb) = 7349 ppm for the TZ2P basis set and σ(Pb) = 8797 ppm for the QZ4P basis set. Calculated $^1J(^{207}Pb,X)$ values are those for the isotope with the highest natural abundance (i.e., ^{35}Cl, ^{79}Br, or ^{127}I spin−spin coupled to ^{207}Pb). [d]Measured at 350 K; spectrum processed with 500 Hz line broadening. [e]A spectrum acquired with SPE and ^{1}H decoupling (70 kHz) had $\nu_{1/2}$ = 3.4(1) kHz. A spectrum acquired with MAS and ^{1}H decoupling had $\nu_{1/2}$ = 2.7(1) kHz.

phase points to subtle ordering of the C−N axis, but the change in dynamics is not dramatic.

For $MAPbI_3$, Kubicki et al.[26] recently reported a reorientational correlation time of 108 ± 18 ps for the MA cation from ^{14}N NMR data at 300 K using a "diffusion-on-a-cone" model. We believe that this value is incompatible with our data and other reported values (see Table 3 of ref 84). Using the ^{14}N T_1 value at 300 K, 0.129 s, and our best estimate of $C_Q(^{14}N)$ = 550 ± 80 kHz, yields a rotational correlation time, τ_2, of 1.7 ± 0.6 ps (see Table 3). Recently Fabini et al. reanalyzed VT ^{1}H NMR T_1 data of Xu et al.[6] and reported a rotational correlation time of approximately 8 ps at room temperature.[27] It is important to recognize that the ^{1}H T_1 data do not yield the same correlation time that the ^{14}N data yield. The ^{14}N relaxation times depend only on fluctuations of the ^{14}N EFG (i.e., motion of the C−N bond axis), while the proton T_1's depend on fluctuations of the ^{1}H−^{1}H dipolar interactions (rotations about the C−N axis, rotations of the C−N axis, and intermolecular dipolar interactions).

Our correlation time for rotation of the C−N axis at 300 K, τ_2, of 1.7 ± 0.6 ps, may be compared to jump times of 3.0 ± 0.7 and 2.6 ± 0.3 ps obtained at room temperature from ultrafast two-dimensional vibrational spectroscopy and molecular dynamics simulations, respectively.[28,85] We suspect that these correlation times correspond to τ_1 values which are longer than τ_2 values. Using elastic and quasi-elastic neutron scattering together with group theoretical analysis, Chen et al.[86] reported characteristic correlation times of 4.70 and 0.82 ps, respectively, for C_4 and C_3 rotations for the MA cation of $MAPbI_3$ at 300 K. Again it appears that their values are for l = 1 that can be converted to τ_2 values by dividing by 3.0; that is $\tau_2(C_4)$ = 1.57 ps and $\tau_2(C_3)$ = 0.27 ps at 300 K, in very good agreement with our values of $\tau_\perp$ = 1.73 ps and $\tau_\parallel$ = 0.19 ps. Likewise, dividing the values obtained by Chen et al. at 350 K by 3.0 yields values of 0.91 and 0.20 ps, respectively, for C_4 and C_3 jumps, which compare well with our values of 0.66 and 0.18 ps, respectively. Considering the uncertainty in the $C_Q(^{14}N)$ and $C_Q(^2H)$ values used to calculate the $\tau_\perp$ and $\tau_\parallel$ values listed in Table 3, the uncertainty in the values may be on the order of 35%. Numerous MD calculations have been reported, and the reader is referred to a recent topical review of perovskite molecular dynamics for reported correlation times and activation energies for $MAPbI_3$.[84]

Table 4 lists the apparent activation energies obtained from fits of our relaxation data. As expected, ^{14}N E_A values are greater than the corresponding ^{2}H values for a given phase, since ^{2}H relaxation probes both motion about the C−N axis (fast, less hindered) and motion of the C−N axis itself, while ^{14}N only probes the latter. Note that, because of the changes taking place in the structure of the tetragonal phase as the temperature increases, the real E_A will likely be changing as well, so although the relaxation data may be fitted linearly to give an "apparent" E_A, this value should be treated with caution. Also, as expected, E_A values are greater for motion in the tetragonal phase than those in the cubic phase. In an early investigation of these compounds in their cubic phases, Xu et al.[6] used ^{1}H NMR relaxation data to determine E_A values ranging from 10.4 to 11.9 kJ·mol^{-1} for the halide perovskite considered in this work; these are similar to those we observe for ^{14}N. Likewise, Maalej et al. reported an activation energy of 10.1 kJ·mol^{-1} for $MAPbCl_3$, based on the results of a VT Raman study.[87]

Using our ^{2}H and ^{14}N T_1 values obtained at 313 K for $MAPbBr_3$, 6.7 and 0.280 s, respectively, from eqs 4−8, we calculate $\tau_\perp$ = 0.743 ps, $\tau_\parallel$ = 0.203 ps, and $\tau_\perp/\tau_\parallel$ = 3.66. The value for $\tau_\perp$ is slightly shorter than that obtained for $MAPbI_3$ in the cubic phase at 330 K; the $\tau_\parallel$ values are the same within experimental error. Our value for $\tau_\perp$ is approximately one-third that reported by Poglitsch and Weber,[4] as expected, since these authors measured τ_1 rather than τ_2. Finally, for pure $MAPbX_3$ films, Selig et al.[85] determined via two-dimensional vibrational spectroscopy that the cation jump times decrease with decreasing size of the halide (3.0 ± 0.7, 1.5 ± 0.3, and 1.2 ± 0.3 ps, respectively, for X = I, Br, and Cl). Given that the $C_Q(^{14}N)$ for $MAPbCl_3$ is almost certainly larger than that for the corresponding bromide or iodide, the T_1 data in Table S3 indicate the same trend in cation jump times (i.e., $\tau_\perp$ decreases on going from X = I to X = Cl in the cubic phase).

^{207}Pb NMR Spectroscopy. Variable temperature ^{207}Pb NMR spectroscopy was undertaken to investigate the response of $\delta(^{207}Pb)$ to temperature. See Table 5 for a summary of the

DOI: 10.1021/acs.jpca.7b11558
J. Phys. Chem. A 2018, 122, 1560−1573

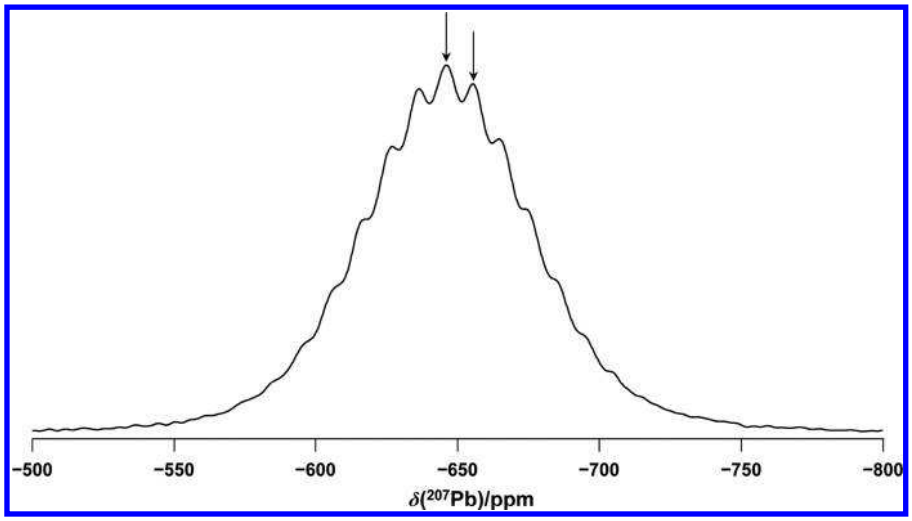

Figure 8. ^{207}Pb NMR spectrum of $CH_3NH_3PbCl_3$ acquired at 4.70 T with an MAS frequency of 3.0 kHz at 293 K. The arrows indicate adjacent peaks in the multiplet attributed to $^1J(^{207}Pb,^{35}Cl)$.

^{207}Pb NMR data and the Supporting Information for a detailed discussion of these results; a brief summary is provided below.

The ^{207}Pb magnetic shielding increases as the temperature decreases for all three perovskite salts in their cubic and tetragonal phases. For X = Br and I, the change in $\delta(^{207}Pb)$ at the cubic ↔ tetragonal phase transition is consistent with the ^{2}H and ^{14}N NMR data discussed above: the trend in chemical shifts is essentially continuous, although the slope of T vs $\delta(^{207}Pb)$ does depend on the phase. It was not possible to investigate this trend for $MAPbCl_3$ because of the narrow temperature range of the tetragonal phase. For the X = Cl and Br salts, there is a dramatic change in $\delta(^{207}Pb)$ at the tetragonal ↔ orthorhombic phase transition temperatures (Figures S11 and S14), although, surprisingly, the shielding decreases upon the transition to the orthorhombic phase for $MAPbCl_3$, but increases with decreasing temperature regardless of phase for the X = Br and I salts. Nevertheless, the large change in $\delta(^{207}Pb)$ at this transition is consistent with the observed changes in $\nu_{QS}(^2H)$ and $\nu_{QS}(^{14}N)$ at these temperatures. Hardware limitations precluded the acquisition of sufficient low-temperature points to discern a trend for the $\delta(^{207}Pb)$ values of $MAPbI_3$, but the one datum acquired for the sample in the orthorhombic phase suggests that the transition to this phase leads to a significant increase in shielding.

Figure S10 illustrates ^{207}Pb NMR spectra for the $MAPbX_3$ salts when these are in their cubic phase (i.e., 293 K for X = Cl or Br and 335 K for X = I). These spectra are notable for their breadths, with $\nu_{1/2}$ values ranging from 3.7 kHz for $MAPbCl_3$ to >20 kHz for $MAPbI_3$ (Table 5). Comparable line widths were reported by Roiland et al. in their investigation of these compounds.[32] Dybowski and co-workers have presented a detailed discussion of factors affecting the ^{207}Pb NMR line widths for spectra of PbI_2.[88] Franssen et al.[36] and Senocrate et al.[34] have studied the temperature dependence of the ^{207}Pb T_2 of $MAPbI_3$. The ^{207}Pb T_2 values are very short, ≈20 μs, and appear to be continuous across the cubic ↔ tetragonal phase transition.[34] Senocrate et al. attributed the short ^{207}Pb T_2 values to strong dipolar coupling and particularly to cross-relaxation to the quadrupolar ^{127}I nuclei which have a magnetogyric ratio similar to that of ^{207}Pb.[34] Given the large values of $^1J(^{207}Pb,^{127}I)$ predicted for $MAPbI_3$ (see Table 5), scalar relaxation of the second kind must also play an important role in contributing to the ^{207}Pb spin−spin relaxation.[54] Rosales et al.[37] also found short ^{207}Pb T_2 values for $MAPbBr_3$ at room temperature (≈87 μs); again on the basis of the calculated values $^1J(^{207}Pb,^{79}Br)$ listed in Table 5, it is clear that scalar relaxation of the second kind must also make a significant contribution to the observed line widths at room temperature. The smaller nuclear quadrupole moments for $^{35/37}$Cl allowed us to obtain a ^{207}Pb NMR spectrum for $MAPbCl_3$ at 4.70 T (Figure 8) which clearly exhibits a splitting pattern that we attribute largely to indirect spin−spin coupling to Cl. Each ^{207}Pb nucleus in this sample is spin−spin coupled to six chlorine nuclei (see Table S2 for the nuclear spin properties of isotopes that factor in the analysis of spectra presented herein). Indirect spin−spin coupling with each chlorine isotope should give rise to a 19-peak multiplet[89] in the ^{207}Pb spectrum, with an approximately 3:1 intensity ratio of the multiplets, based on the natural abundance of the isotope giving rise to the multiplet. The splitting pattern observed in Figure 8 is attributed to spin−spin coupling to ^{35}Cl since this isotope has the greater natural abundance. The peak−peak separation measured near the center of the spectrum suggests that $^1J(^{207}Pb,^{35}Cl) = 400 \pm 40$ Hz; a large error of ±10% has been assigned due to complications arising from the perturbation of the Zeeman splitting arising from nuclear quadrupolar interactions with the six neighboring $^{35/37}$Cl nuclei.[90] Note that the ^{35}Cl NQR frequency is approximately 8.1 MHz for $MAPbCl_3$ in its cubic phase.[6]

Although the two magnetically active isotopes of bromine are also spin-3/2 nuclei, as discussed above, it is not possible to resolve any splitting due to $^1J(^{207}Pb,^{79/81}Br)$ for $MAPbBr_3$. The much greater nuclear quadrupole moments for the two bromine isotopes means that they are expected to have much larger nuclear quadrupolar coupling (NQR frequencies of 70.451 and 58.842 MHz, respectively, were reported for the ^{79}Br and ^{81}Br NQR spectra of $MAPbBr_3$, measured at 298 K)[6] giving rise to an uneven splitting pattern in the ^{207}Pb NMR spectra, further complicating the analysis. Likewise, splitting patterns due to $^1J(^{207}Pb,^{127}I)$ are not observed for ^{207}Pb NMR spectra for $MAPbI_3$, as discussed above.

Table 5 summarizes calculated $^1J(^{207}Pb,X)$ values obtained using a basic PbX_6 model structure. These calculations yield a reasonable value for $^1J(^{207}Pb,^{35}Cl)$ for $MAPbCl_3$ and suggest

DOI: 10.1021/acs.jpca.7b11558
J. Phys. Chem. A 2018, 122, 1560−1573

that much larger values are expected for the X = Br and I perovskites. Table 5 also summarizes the calculated reduced coupling constant, ^1K(Pb,X), which factors out the effect of the magnetogyric ratios from the observed spin−spin coupling. The calculated ^1K values reproduce the expected trend, with ^1K(Pb,Cl) < ^1K(Pb,Br) < ^1K(Pb,I).[91,92]

CONCLUSIONS

As demonstrated more than 30 years ago, solid-state NMR spectroscopy is an ideal tool for characterizing phase transitions and dynamics in $MAPbX_3$ perovskites and in related photovoltaic materials. Modern instrumentation and computational resources have permitted a more careful NMR investigation of the $MAPbX_3$ salts. Consistent with structural data, variable temperature NMR data show that the ^{2}H and ^{14}N spin−lattice relaxation times for $MAPbI_3$, although sensitive to temperature, are continuous through the cubic ↔ tetragonal phase transitions. ^{2}H T_1 values for $CH_3ND_3PbBr_3$ are also continuous across this transition. Likewise, the ^{207}Pb chemical shifts are very sensitive to temperature, but there are no large discontinuities in the observed ^{207}Pb chemical shifts at the cubic ↔ tetragonal phase transition. Although some investigators have suggested that the MA cation may reside exclusively in or near the *ab*-plane for these salts in the tetragonal phase, our ^{2}H data demonstrate that, although the cation favors this plane, it must spend some time parallel to the *c*-axis; a model has been proposed to describe this behavior. On the basis of our T_1 data it is difficult to envision a model where the motion of the C−N axis of the MA cation immediately below the cubic ↔ tetragonal phase transition is confined to a plane or diffusion about a cone. Finally, we show that the breadth of the ^{207}Pb NMR spectra for $MAPbCl_3$ is primarily due to spin−spin coupling to $^{35/37}$Cl, with $^1J(^{207}Pb,^{35}Cl) \approx 400$ Hz; DFT calculations suggest larger $^1J(^{207}Pb,X)$ values for the X = Br and I salts.

ASSOCIATED CONTENT

Supporting Information

The Supporting Information is available free of charge on the ACS Publications website at DOI: 10.1021/acs.jpca.7b11558.

Summary of ν_{QS} values for MAX salts, nuclear spin properties for nuclei of interest, ^{2}H and ^{14}N T_1 values, ^{2}H quadrupolar splitting plotted vs $1000/T$, $\ln(T_1)$ plotted as a function of $1000/T$, further ^{2}H and ^{14}N NMR spectra, detailed discussion of ^{207}Pb NMR results (PDF)

AUTHOR INFORMATION

ORCID

Guy M. Bernard: 0000-0003-1507-6705
Roderick E. Wasylishen: 0000-0003-4150-3651
Victor Terskikh: 0000-0003-1514-2610
Jillian M. Buriak: 0000-0002-9567-4328

Notes

The authors declare no competing financial interest.

ACKNOWLEDGMENTS

We thank Dr. Mike Lumsden and Mr. J. Bruce Macdonald (Dalhousie University), for preliminary work on this project, as well as Mr. Abdelrahman Askar and Mr. Aaron Dong for their assistance in the preparation of some materials. We are grateful to Drs. Bob McDonald and Mike Ferguson for helpful discussions on X-ray data, to Dr. Klaus Eichele for many useful discussions, to Ms. Michelle Ha for her help in organizing the literature and to Mr. Eric Wasylishen for his assistance with the analysis of some data. Access to the 21.1 T NMR spectrometer was provided by the National Ultrahigh-Field NMR Facility for Solids (Ottawa, Canada), a national research facility funded by a consortium of Canadian Universities, supported by the National Research Council Canada and Bruker BioSpin, and managed by the University of Ottawa (http://nmr900.ca). Funding is provided by the Natural Sciences and Engineering Research Council (NSERC) of Canada and SABIC. R.E.W. is grateful to his former colleague and friend the late Prof. Osvald Knop for introducing him to these intriguing compounds more than 30 years ago.

REFERENCES

(1) Weber, D. CH_3NH_3PbX3, ein Pb(II)-System mit Kubischer Perowskitstruktur. *Z. Naturforsch., B: J. Chem. Sci.* **1978**, *33*, 1443−1445.

(2) Knop, O.; Wasylishen, R. E.; White, M. A.; Cameron, T. S.; Van Oort, M. J. M. Alkylammonium Lead Halides. Part. 2. $CH_3NH_3PbX_3$ (X = Cl, Br, I) Perovskites: Cuboctahedral Halide Cages with Isotropic Cation Reorientation. *Can. J. Chem.* **1990**, *68*, 412−422.

(3) Wasylishen, R. E.; Knop, O.; Macdonald, J. B. Cation Rotation in Methylammonium Lead Halides. *Solid State Commun.* **1985**, *56*, 581−582.

(4) Poglitsch, A.; Weber, D. Dynamic Disorder in Methylammoniumtrihalogenoplumbates (II) Observed by Millimeter-Wave Spectroscopy. *J. Chem. Phys.* **1987**, *87*, 6373−6378.

(5) Onoda-Yamamuro, N.; Matsuo, T.; Suga, H. Calorimetric and IR Spectroscopic Studies of Phase Transitions in Methylammonium Trihalogenoplumbates (II). *J. Phys. Chem. Solids* **1990**, *51*, 1383−1395.

(6) Xu, Q.; Eguchi, T.; Nakayama, H.; Nakamura, N.; Kishita, M. Molecular Motions and Phase Transitions in Solid $CH_3NH_3PbX_3$ (X = Cl, Br, I) as Studied by NMR and NQR. *Z. Naturforsch., A: Phys. Sci.* **1991**, *46*, 240−246.

(7) Weller, M. T.; Weber, O. J.; Henry, P. F.; Di Pumpo, A. M.; Hansen, T. C. Complete Structure and Cation Orientation in the Perovskite Photovoltaic Methylammonium Lead Iodide Between 100 and 352 K. *Chem. Commun.* **2015**, *51*, 4180−4183.

(8) Swainson, I. P.; Hammond, R. P.; Soullière, C.; Knop, O.; Massa, W. Phase Transitions in the Perovskite Methylammonium Lead Bromide, $CH_3ND_3PbBr_3$. *J. Solid State Chem.* **2003**, *176*, 97−104.

(9) Chi, L.; Swainson, I.; Cranswick, L.; Her, J.-H.; Stephens, P.; Knop, O. The Ordered Phase of Methylammonium Lead Chloride $CH_3ND_3PbCl_3$. *J. Solid State Chem.* **2005**, *178*, 1376−1385.

(10) Mashiyama, H.; Kawamura, Y.; Magome, E.; Kubota, Y. Displacive Character of the Cubic-Tetragonal Transition in $CH_3NH_3PbX_3$. *J. Korean Phys. Soc.* **2003**, *42*, S1026−S1029.

(11) Kawamura, Y.; Mashiyama, H.; Hasebe, K. Structural Study on Cubic-Tetragonal Transition of $CH_3NH_3PbI_3$. *J. Phys. Soc. Jpn.* **2002**, *71*, 1694−1697.

(12) Stoumpos, C. C.; Malliakas, C. D.; Kanatzidis, M. G. Semiconducting Tin and Lead Iodide Perovskites with Organic Cations: Phase Transitions, High Mobilities, and Near-Infrared Photoluminescent Properties. *Inorg. Chem.* **2013**, *52*, 9019−9038.

(13) Baikie, T.; Barrow, N. S.; Fang, Y.; Keenan, P. J.; Slater, P. R.; Piltz, R. O.; Gutmann, M.; Mhaisalkar, S. G.; White, T. J. A Combined Single Crystal Neutron/X-Ray Diffraction and Solid-State Nuclear Magnetic Resonance Study of the Hybrid Perovskites $CH_3NH_3PbX_3$ (X = I, Br and Cl). *J. Mater. Chem. A* **2015**, *3*, 9298−9307.

(14) Ren, Y.; Oswald, I. W. H.; Wang, X.; McCandless, G. T.; Chan, J. Y. Orientation of Organic Cations in Hybrid Inorganic-Organic Perovskite $CH_3NH_3PbI_3$ from Subatomic Resolution Single Crystal Neutron Diffraction Studies. *Cryst. Growth Des.* **2016**, *16*, 2945−2951.

DOI: 10.1021/acs.jpca.7b11558
J. Phys. Chem. A 2018, 122, 1560−1573

(15) Whitfield, P. S.; Herron, N.; Guise, W. E.; Page, K.; Cheng, Y. Q.; Milas, I.; Crawford, M. K. Structures, Phase Transitions and Tricritical Behavior of the Hybrid Perovskite Methyl Ammonium Lead Iodide. *Sci. Rep.* **2016**, *6*, 35685.
(16) Mitzi, D. B. Synthesis, Structure, and Properties of Organic-Inorganic Perovskites and Related Materials. *Prog. Inorg. Chem.* **1999**, *48*, 1−121.
(17) Kojima, A.; Teshima, K.; Shirai, Y.; Miyasaka, T. Organometal Halide Perovskites as Visible-Light Sensitizers for Photovoltaic Cells. *J. Am. Chem. Soc.* **2009**, *131*, 6050−6051.
(18) Rosales, B. A.; Hanrahan, M. P.; Boote, B. W.; Rossini, A. J.; Smith, E. A.; Vela, J. Lead Halide Perovskites: Challenges and Opportunities in Advanced Synthesis and Spectroscopy. *ACS Energy Lett.* **2017**, *2*, 906−914.
(19) Herz, L. M. Charge-Carrier Mobilities in Metal Halide Perovskites: Fundamental Mechanisms and Limits. *ACS Energy Lett.* **2017**, *2*, 1539−1548.
(20) Hu, H.; Dong, B.; Zhang, W. Low-Toxic Metal Halide Perovskites: Opportunities and Future Challenges. *J. Mater. Chem. A* **2017**, *5*, 11436−11449.
(21) Yang, S.; Fu, W.; Zhang, Z.; Chen, H.; Li, C.-Z. Recent Advances in Perovskite Solar Cells: Efficiency, Stability and Lead-Free Perovskite. *J. Mater. Chem. A* **2017**, *5*, 11462−11482.
(22) Saliba, M.; Matsui, T.; Seo, J.-Y.; Domanski, K.; Correa-Baena, J.-P.; Nazeeruddin, M. K.; Zakeeruddin, S. M.; Tress, W.; Abate, A.; Hagfeldt, A.; et al. Cesium-Containing Triple Cation Perovskite Solar Cells: Improved Stability, Reproducibility and High Efficiency. *Energy Environ. Sci.* **2016**, *9*, 1989−1997.
(23) Bi, D.; Tress, W.; Dar, M. I.; Gao, P.; Luo, J.; Renevier, C.; Schenk, K.; Abate, A.; Giordano, F.; Correa Baena, J.-P.; et al. Efficient Luminescent Solar Cells Based on Tailored Mixed-Cation Perovskites. *Sci. Adv.* **2016**, *2*, e1501170.
(24) Yang, W. S.; Noh, J. H.; Jeon, N. J.; Kim, Y. C.; Ryu, S.; Seo, J.; Seok, S. I. High-Performance Photovoltaic Perovskite Layers Fabricated Through Intramolecular Exchange. *Science* **2015**, *348*, 1234−1237.
(25) Gong, J.; Yang, M.; Ma, X.; Schaller, R. D.; Liu, G.; Kong, L.; Yang, Y.; Beard, M. C.; Lesslie, M.; Dai, Y.; et al. Electron−Rotor Interaction in Organic−Inorganic Lead Iodide Perovskites Discovered by Isotope Effects. *J. Phys. Chem. Lett.* **2016**, *7*, 2879−2887.
(26) Kubicki, D. J.; Prochowicz, D.; Hofstetter, A.; Péchy, P.; Zakeeruddin, S. M.; Grätzel, M.; Emsley, L. Cation Dynamics in Mixed-Cation $(MA)_x(FA)_{1-x}PbI_3$ Hybrid Perovskites from Solid-State NMR. *J. Am. Chem. Soc.* **2017**, *139*, 10055−10061.
(27) Fabini, D. H.; Siaw, T. A.; Stoumpos, C. C.; Laurita, G.; Olds, D.; Page, K.; Hu, J. G.; Kanatzidis, M. G.; Han, S.; Seshadri, R. Universal Dynamics of Molecular Reorientation in Hybrid Lead Iodide Perovskites. *J. Am. Chem. Soc.* **2017**, *139*, 16875−16884.
(28) Bakulin, A. A.; Selig, O.; Bakker, H. J.; Rezus, Y. L. A.; Müller, C.; Glaser, T.; Lovrincic, R.; Sun, Z.; Chen, Z.; Walsh, A.; et al. Real-Time Observation of Organic Cation Reorientation in Methylammonium Lead Iodide Perovskites. *J. Phys. Chem. Lett.* **2015**, *6*, 3663−3669.
(29) Frost, J. M.; Walsh, A. What is Moving in Hybrid Halide Solar Cells? *Acc. Chem. Res.* **2016**, *49*, 528−535.
(30) Zhu, H.; Miyata, K.; Fu, Y.; Wang, J.; Joshi, P. P.; Niesner, D.; Williams, K. W.; Jin, S.; Zhu, X.-Y. Screening in Crystalline Liquids Protects Energetic Carriers in Hybrid Perovskites. *Science* **2016**, *353*, 1409−1413.
(31) Li, Y.; Behtash, M.; Wong, J.; Yang, K. Enhancing Ferroelectric Dipole Ordering in Organic-Inorganic Hybrid Perovskite $CH_3NH_3PbI_3$: Strain and Doping Engineering. *J. Phys. Chem. C* **2018**, *122*, 177−184.
(32) Roiland, C.; Trippé-Allard, G.; Jemli, K.; Alonso, B.; Ameline, J.-C.; Gautier, R.; Bataille, T.; Le Pollès, L.; Deleporte, E.; Even, J.; et al. Multinuclear NMR as a Tool for Studying Local Order and Dynamics in $CH_3NH_3PbX_3$ (X = Cl, Br, I) Hybrid Perovskites. *Phys. Chem. Chem. Phys.* **2016**, *18*, 27133−27142.
(33) Kubicki, D. J.; Prochowicz, D.; Hofstetter, A.; Zakeeruddin, S. M.; Grätzel, M.; Emsley, L. Phase Segregation in Cs-, Rb- and K-Doped Mixed-Cation $(MA)_xFA_{1-x}PbI_3$ Hybrid Perovskites from Solid-State NMR. *J. Am. Chem. Soc.* **2017**, *139*, 14173−14180.
(34) Senocrate, A.; Moudrakovski, I.; Kim, G. Y.; Yang, T.-Y.; Gregori, G.; Grätzel, M.; Maier, J. The Nature of Ion Conduction in Methylammonium Lead Iodide: A Multimethod Approach. *Angew. Chem., Int. Ed.* **2017**, *56*, 7755−7759.
(35) Askar, A. M.; Bernard, G. M.; Wiltshire, B.; Shankar, K.; Michaelis, V. K. Multinuclear Magnetic Resonance Tracking of Hydro, Thermal, and Hydrothermal Decomposition of $CH_3NH_3PbI_3$. *J. Phys. Chem. C* **2017**, *121*, 1013−1024.
(36) Franssen, W. M. J.; van Es, S. G. D.; Dervişoğlu, R.; de Wijs, G. A.; Kentgens, A. P. M. Symmetry, Dynamics, and Defects in Methylammonium Lead Halide Perovskites. *J. Phys. Chem. Lett.* **2017**, *8*, 61−66.
(37) Rosales, B. A.; Men, L.; Cady, S. D.; Hanrahan, M. P.; Rossini, A. J.; Vela, J. Persistent Dopants and Phase Segregation in Organolead Mixed-Halide Perovskites. *Chem. Mater.* **2016**, *28*, 6848−6859.
(38) Bernard, G. M.; Goyal, A.; Miskolzie, M.; McKay, R.; Wu, Q.; Wasylishen, R. E.; Michaelis, V. K. Methylammonium Lead Chloride: A Sensitive Sample for an Accurate NMR Thermometer. *J. Magn. Reson.* **2017**, *283*, 14−21.
(39) Pyykkö, P. Year-2008 Nuclear Quadrupole Moments. *Mol. Phys.* **2008**, *106*, 1965−1974.
(40) Ratcliffe, C. I. Phase Behaviour and Dynamics in Ethylammonium Halide Salts. *Can. J. Chem.* **2004**, *82*, 1517−1526.
(41) Jelinski, L. W. Solid State Deuterium NMR Studies of Polymer Chain Dynamics. *Annu. Rev. Mater. Sci.* **1985**, *15*, 359−377.
(42) Spiess, H. W. Molecular Dynamics of Solid Polymers as Revealed by Deuteron NMR. *Colloid Polym. Sci.* **1983**, *261*, 193−209.
(43) O'Dell, L. A.; Ratcliffe, C. I. Quadrupolar NMR to Investigate Dynamics in Solid Materials. In *Encyclopedia of Magnetic Resonance*; Harris, R. K., Wasylishen, R. E., Eds.; John Wiley: Chichester, U.K., 2012; Vol. 7, pp 3814−3829. DOI: 10.1002/9780470034590.emrstm1209.
(44) Schmidt-Rohr, K.; Spiess, H. W. *Multidimensional Solid-State NMR and Polymers*; Academic Press: London, 1994.
(45) Boden, N. NMR Studies of Plastic Crystals. In *The Plastically Crystalline State. (Orientationally Disordered Crystals)*; Sherwood, J. N., Ed.; John Wiley & Sons: Chichester, U.K., 1979; Chapter 5, pp 147−214.
(46) Bryce, D. L.; Bernard, G. M.; Gee, M.; Lumsden, M. D.; Eichele, K.; Wasylishen, R. E. Practical Aspects of Modern Routine Solid-State Multinuclear Magnetic Resonance Spectroscopy: One-Dimensional Experiments. *Can. J. Anal. Sci. Spectrosc.* **2001**, *46*, 46−82.
(47) Wasylishen, R. E. A Multinuclear Magnetic Resonance Study of Methylammonium Nitrate. *Can. J. Chem.* **1986**, *64*, 773−776.
(48) Lehn, J. M.; Kintzinger, J. P. Nitrogen-14 Nuclear Quadrupole Effect. In *Nitrogen NMR*; Witanowski, M., Webb, G. A., Eds.; Plenum Press: New York, 1973; Chapter 3, pp 79−161.
(49) Abragam, A. *Principles of Magnetic Resonance*; Oxford University Press: Oxford, 1961; Chapter VIII, pp 364−353.
(50) Farrar, T. C.; Becker, E. D. *Pulse and Fourier Transform NMR, Introduction to Theory and Methods*; Academic Press: New York, 1971; Section 4.4, pp 58−59.
(51) Harris, R. K. *Nuclear Magnetic Resonance Spectroscopy*; Longman Scientific & Technical: Essex, U.K., 1986; Chapter 5B, pp 131−143.
(52) Wasylishen, R. E. NMR Relaxation and Dynamics. In *NMR Spectroscopy Techniques*, 2nd ed.; Bruch, M. D., Ed.; Practical Spectroscopy Series 21; Marcel Dekker: New York, 1996; Chapter 3, pp 105−144.
(53) Stoppa, A.; Nazet, A.; Buchner, R.; Thoman, A.; Walther, M. Dielectric Response and Collective Dynamics of Acetonitrile. *J. Mol. Liq.* **2015**, *212*, 963−968.
(54) Spiess, H. W. Rotation of Molecules and Nuclear Spin Relaxation. In *NMR Basic Principles and Progress*; Springer-Verlag: Berlin, 1978; Vol. *15*, pp 55−214.

DOI: 10.1021/acs.jpca.7b11558
J. Phys. Chem. A 2018, 122, 1560−1573

(55) Carrington, A.; McLachlan, A. D. *Introduction to Magnetic Resonance*; Halsted Press: New York, 1967; Chapter 11, pp 176−203.
(56) Woessner, D. E. Molecular Reorientation in Liquids. Deuteron Quadrupole Relaxation in Liquid Deuterium Oxide and Perdeuterobenzene. *J. Chem. Phys.* **1964**, *40*, 2341−2348.
(57) Woessner, D. E.; Snowden, B. S., Jr.; Strom, E. T. A Study of Molecular Re-Orientation in Liquid Acetonitrile by Nuclear Spin-Lattice Relaxation. *Mol. Phys.* **1968**, *14*, 265−273.
(58) Noggle, J. H.; Schirmer, R. E. *The Nuclear Overhauser Effect, Chemical Applications*; Academic Press: New York, 1971; Chapter 2, pp 21−43.
(59) Borsa, F. Phase Transitions and Critical Phenomena in Solids. In *Encyclopedia of Magnetic Resonance*; Harris, R. K., Wasylishen, R. E., Eds.; John Wiley & Sons: Chichester, U.K., 2012; Vol. *6*, pp 3364−3372. DOI: 10.1002/9780470034590.emrstm0390.
(60) Jeffrey, K. R.; Penner, G. H. Structural Phase Transitions. In *NMR Crystallography*; Harris, R. K., Wasylishen, R. E., Duer, M. J., Eds.; John Wiley: Chichester, U.K., 2009; Chapter 26, pp 387−413. DOI: 10.1002/9780470034590.emrstm1051.
(61) O'Dell, L. A.; Rossini, A. J.; Schurko, R. W. *Chem. Phys. Lett.* **2009**, *468*, 330−335.
(62) Schurko, R. W. Acquisition of Wideline Solid-State NMR Spectra of Quadrupolar Nuclei. In *NMR of Quadrupolar Nuclei in Solid Materials*; Wasylishen, R. E., Ashbrook, S. E., Wimperis, S., Eds.; John Wiley & Sons: Chichester, U.K., 2012; Chapter 5, pp 77−93.
(63) Neue, G.; Dybowski, C.; Smith, M. L.; Hepp, M. A.; Perry, D. L. Determination of $^{207}Pb^{2+}$ Chemical Shift Tensors from Precise Powder Lineshape Analysis. *Solid State Nucl. Magn. Reson.* **1996**, *6*, 241−250.
(64) van Gorkom, L. C. M.; Hook, J. M.; Logan, M. B.; Hanna, J. V.; Wasylishen, R. E. Solid-State Lead-207 NMR of Lead(II) Nitrate: Localized Heating Effects at High Magic Angle Spinning Speeds. *Magn. Reson. Chem.* **1995**, *33*, 791−795.
(65) Dybowski, C.; Neue, G. Solid State ^{207}Pb NMR Spectroscopy. *Prog. Nucl. Magn. Reson. Spectrosc.* **2002**, *41*, 153−170.
(66) ADF2012; SCM; Theoretical Chemistry, Vrije Universiteit: Amsterdam, The Netherlands. http://www.scm.com.
(67) Fonseca Guerra, C.; Snijders, J. G.; te Velde, G.; Baerends, E. J. Towards an Order-*N* DFT Method. *Theor. Chem. Acc.* **1998**, *99*, 391−403.
(68) te Velde, G.; Bickelhaupt, F. M.; Baerends, E. J.; Fonseca Guerra, C.; van Gisbergen, S. J. A.; Snijders, J. G.; Ziegler, T. Chemistry with ADF. *J. Comput. Chem.* **2001**, *22*, 931−967.
(69) Wolff, S. K.; Ziegler, T.; van Lenthe, E.; Baerends, E. J. Density Functional Calculations of Nuclear Magnetic Shieldings Using the Zeroth-Order Regular Approximation (ZORA) for Relativistic Effects: ZORA Nuclear Magnetic Resonance. *J. Chem. Phys.* **1999**, *110*, 7689−7698.
(70) van Lenthe, E.; Baerends, E. J.; Snijders, J. G. Relativistic Regular Two-Component Hamiltonians. *J. Chem. Phys.* **1993**, *99*, 4597−4610.
(71) van Lenthe, E.; Baerends, E. J.; Snijders, J. G. Relativistic Total Energy Using Regular Approximations. *J. Chem. Phys.* **1994**, *101*, 9783−9792.
(72) van Lenthe, E.; Ehlers, A.; Baerends, E.-J. Geometry Optimizations in the Zero Order Regular Approximation for Relativistic Effects. *J. Chem. Phys.* **1999**, *110*, 8943−8953.
(73) Oyamada, T.; Iijima, T.; Kimura, M. Molecular Structure and Phase-Shift of Tetramethyllead as Studied by Gas Electron Diffraction. *Bull. Chem. Soc. Jpn.* **1971**, *44*, 2638−2642.
(74) Yin, T.; Fang, Y.; Fan, X.; Zhang, B.; Kuo, J.-L.; White, T. J.; Chow, G. M.; Yan, J.; Shen, Z. X. Hydrogen-Bonding Evolution During the Polymorphic Transformations in $CH_3NH_3PbBr_3$: Experiment and Theory. *Chem. Mater.* **2017**, *29*, 5974−5981.
(75) Jurga, S.; Spiess, H. W. Interrelation Between Molecular Motions and Phase Transitions in Monomethylammonium Perchlorate. A Study by DSC, Proton, and Deuteron NMR. *Z. Naturforsch. A* **1985**, *40*, 602−610.
(76) Jakobsen, H. J.; Hove, A. R.; Hazell, R. G.; Bildsøe, H.; Skibsted, J. Solid-State ^{14}N MAS NMR of Ammonium Ions as a Spy to Structural Insights for Ammonium Salts. *Magn. Reson. Chem.* **2006**, *44*, 348−356.
(77) Mattoni, A.; Filippetti, A.; Saba, M. I.; Delugas, P. Methylammonium Rotational Dynamics in Lead Halide Perovskite by Classical Molecular Dynamics: the Role of Temperature. *J. Phys. Chem. C* **2015**, *119*, 17421−17428.
(78) Brivio, F.; Walker, A. B.; Walsh, A. Structural and Electronic Properties of Hybrid Perovskites for High-Efficiency Thin-Film Photovoltaics from First-Principles. *APL Mater.* **2013**, *1*, 042111.
(79) Frost, J. M.; Butler, K. T.; Walsh, A. Molecular Ferroelectric Contributions to Anomalous Hysteresis in Hybrid Perovskite Solar Cells. *APL Mater.* **2014**, *2*, 081506.
(80) Leguy, A. M. A.; Frost, J. M.; McMahon, A. P.; Garcia Sakai, V.; Kockelmann, W.; Law, C.; Li, X.; Foglia, F.; Walsh, A.; O'Regan, B. C.; et al. The Dynamics of Methylammonium Ions in Hybrid Organic-Inorganic Perovskite Solar Cells. *Nat. Commun.* **2015**, *6*, 7124.
(81) Lee, J.-H.; Bristowe, N. C.; Bristowe, P. D.; Cheetham, A. K. Role of Hydrogen-Bonding and its Interplay with Octahedral Tilting in $CH_3NH_3PbI_3$. *Chem. Commun.* **2015**, *51*, 6434−6437.
(82) Berne, B. J.; Pecora, R. *Dynamic Light Scattering With Applications to Chemistry, Biology and Physics*; John Wiley & Sons: New York, 1976.
(83) Polatin, P.; Barbara, T.; Dailey, B. P. The Determination of the ^{14}N Nuclear Quadrupole Coupling Constant for the Methylammonium Ion in a Liquid-Crystal Solution. *J. Magn. Reson.* **1982**, *47*, 148−150.
(84) Mattoni, A.; Filippetti, A.; Caddeo, C. Modeling Hybrid Perovskites by Molecular Dynamics. *J. Phys.: Condens. Matter* **2017**, *29*, 043001.
(85) Selig, O.; Sadhanala, A.; Müller, C.; Lovrincic, R.; Chen, Z.; Rezus, Y. L. A.; Frost, J. M.; Jansen, T. L. C.; Bakulin, A. A. Organic Cation Rotation and Immobilization in Pure and Mixed Methylammonium Lead-Halide Perovskites. *J. Am. Chem. Soc.* **2017**, *139*, 4068−4074.
(86) Chen, T.; Foley, B. J.; Ipek, B.; Tyagi, M.; Copley, J. R. D.; Brown, C. M.; Choi, J. J.; Lee, S.-H. Rotational Dynamics of Organic Cations in the $CH_3NH_3PbI_3$ Perovskite. *Phys. Chem. Chem. Phys.* **2015**, *17*, 31278−31286.
(87) Maalej, A.; Abid, Y.; Kallel, A.; Daoud, A.; Lautié, A.; Romain, F. Phase Transitions and Crystal Dynamics in the Cubic Perovskite $CH_3NH_3PbCl_3$. *Solid State Commun.* **1997**, *103*, 279−284.
(88) Taylor, R. E.; Beckmann, P. A.; Bai, S.; Dybowski, C. ^{127}I and ^{207}Pb Solid State NMR Spectroscopy and Nuclear Spin Relaxation in PbI_2: A Preliminary Study. *J. Phys. Chem. C* **2014**, *118*, 9143−9153.
(89) Lash, T. D.; Lash, S. S. The Use of Pascal-Like Triangles in Describing First-Order NMR Coupling Patterns. *J. Chem. Educ.* **1987**, *64*, 315.
(90) Grondona, P.; Olivieri, A. C. Quadrupole Effects in Solid-State NMR Spectra of Spin-1/2 Nuclei: a Perturbation Approach. *Concepts Magn. Reson.* **1993**, *5*, 319−339.
(91) Bryce, D. L.; Wasylishen, R. E.; Autschbach, J.; Ziegler, T. Periodic Trends in Indirect Nuclear Spin-Spin Coupling Tensors: Relativistic Density Functional Calculations for Interhalogen Diatomics. *J. Am. Chem. Soc.* **2002**, *124*, 4894−4900.
(92) Jameson, C. J.; Gutowsky, H. S. Systematic Trends in the Coupling Constants of Directly Bonded Nuclei. *J. Chem. Phys.* **1969**, *51*, 2790−2803.

DOI: 10.1021/acs.jpca.7b11558
J. Phys. Chem. A 2018, 122, 1560−1573